NACA RM L51A26

NACA

RESEARCH MEMORANDUM

INVESTIGATION AT LOW SPEED OF THE EFFECTIVENESS AND HINGE MOMENTS OF A CONSTANT-CHORD AILAVATOR ON A LARGE-SCALE TRIANGULAR WING WITH SECTION MODIFICATION

By John G. Hawes and Ralph W. May, Jr.

Langley Aeronautical Laboratory
Langley Field, Va.

NATIONAL ADVISORY COMMITTEE
FOR AERONAUTICS

WASHINGTON
April 24, 1951

NATIONAL ADVISORY COMMITTEE FOR AERONAUTICS

RESEARCH MEMORANDUM

INVESTIGATION AT LOW SPEED OF THE EFFECTIVENESS AND HINGE MOMENTS OF A CONSTANT-CHORD AILAVATOR ON A LARGE-SCALE TRIANGULAR WING WITH SECTION MODIFICATION

By John G. Hawes and Ralph W. May, Jr.

SUMMARY

An investigation has been conducted in the Langley full-scale tunnel to determine the low-speed longitudinal, lateral, and hinge-moment control characteristics of a basic 60° delta wing of aspect ratio 2.31 with 10-percent-thick biconvex symmetrical airfoil sections. The wing was also tested in an altered condition with a nose glove employing NACA 65-010 section ordinates. The wing was equipped on the left semispan with a constant-chord plain semispan ailavator having two segments.

The results indicate that the characteristic force breaks caused by a separation vortex on the basic sharp-edged airfoil were eliminated by installing an NACA 65-010 nose glove. The effectiveness and hinge moments for the full semispan ailavator for both wings represent the sum of the characteristics of the two segments. The leading-edge separation vortex on the sharp-edged wing introduced large hinge-moment discontinuities with large ailavator deflections.

INTRODUCTION

Previous pressure-distribution and flow investigations of triangular wings (references 1, 2, and 3) have shown leading-edge separation with an accompanying strong vortex flow for wings with sharp-edged airfoils, but the effect of the vortex decreased for the wings having airfoil sections with increasing nose radii. In fact, the large-scale triangular wing of reference 1 and the small-scale triangular wing of reference 4, both with rounded leading edges, showed trailing-edge separation of the type normally expected for conventional wings.

In the flow investigation of a zero-taper-ratio wing, reported in reference 3, it was shown that the separation vortices increased in size and intensity as they swept progressively from the leading edge inboard toward the plane of symmetry with increased angle of attack. The progression of this type of flow over the tip sections and wing trailing edge would be expected to influence the control characteristics of trailing-edge flaps or ailavators, in view of the varied loading of the sections.

The present tests were conducted in the Langley full-scale tunnel to investigate the effects of the vortex flow on the effectiveness and hinge-moment characteristics of outboard, inboard, and full-semispan constant-chord ailavators on the large-scale triangular wing of reference 5.

In an attempt to alleviate the leading-edge separation and vortex flow, the nose section of the basic wing was altered by installing a glove incorporating NACA 65-010 section ordinates parallel to the free stream over the forward 10 percent of the chord and faired to the wing at approximately the 50-percent-chord line.

COEFFICIENTS AND SYMBOLS

The data are presented as standard NACA coefficients of forces and moments. The data are referred to a set of axes coinciding with the wind axes, and the origin was located at the quarter chord of the mean aerodynamic chord.

C_L wing lift coefficient $\left(\frac{L}{qS}\right)$

C_D drag coefficient $\left(\frac{D}{qS}\right)$

C_m pitching-moment coefficient $\left(\frac{M}{q\bar{c}S}\right)$

C_h hinge-moment coefficient $\left(\frac{H}{q\bar{c}_a{}^2 b_a}\right)$

C_l rolling-moment coefficient $\left(\frac{L'}{qbS}\right)$

C_n yawing-moment coefficient $\left(\frac{N}{qbS}\right)$

$\left(C_{L_\delta}\right)_L = \frac{\partial C_L}{\partial \delta_L}$ rate of change of lift coefficient with left ailavator deflection at $\delta_L = 0$, per degree

$\left(C_{m_\delta}\right)_L = \frac{\partial C_m}{\partial \delta_L}$ rate of change of pitching-moment coefficient with left ailavator deflection at $\delta_L = 0$, per degree

$\left(C_{h_\delta}\right)_L = \frac{\partial C_h}{\partial \delta_L}$ rate of change of hinge-moment coefficient with left ailavator deflection at $\delta_L = 0$, per degree

$\left(C_{l_\delta}\right)_L = \frac{\partial C_l}{\partial \delta_L}$ rate of change of rolling-moment coefficient with left ailavator deflection at $\delta_L = 0$, per degree

$\left(C_{n_\delta}\right)_L = \frac{\partial C_n}{\partial \delta_L}$ rate of change of yawing-moment coefficient with left ailavator deflection at $\delta_L = 0$, per degree

L'	rolling moment, foot-pounds
M	pitching moment, foot-pounds
N	yawing moment, foot-pounds
H	hinge moment, foot-pounds
L	lift, pounds
S	area of the wing, square feet
V	airspeed, feet per second
D	total drag, pounds
b	wing span, feet
y	distance along lateral axis, feet
c	wing chord, feet
$\bar{c}$	mean aerodynamic chord, M.A.C., feet $\left(\frac{2}{S}\int_0^{b/2} c^2 dy\right)$
$\bar{c}_a$	ailavator root-mean-square chord, feet
b_a	ailavator span, feet

q	dynamic pressure $\left(\frac{1}{2}\rho V^2\right)$, pounds per square foot
α	angle of attack of the wing chord line, degrees
ρ	mass density of air, slugs per cubic foot
δ_L	angle of left ailavator from wing chord line, positive down, degrees

Subscripts:

L	left semispan
i	inboard ailavator
o	outboard ailavator

MODEL

The geometric characteristics of the basic sharp leading-edge wing having 60° leading-edge sweep and 10-percent-thick symmetrical biconvex airfoil sections parallel to the plane of symmetry are given in figure 1. The wing has an area of 231 square feet and an aspect ratio of 2.31. Further description of the wing is given in reference 5.

The round-nose configuration was formed by attaching an NACA 65-010 airfoil section nose glove to the basic wing. A true section was formed to the 10-percent-chord line and was arbitrarily faired from this station to the basic wing at approximately the 50-percent-chord line. A gap was provided in the glove on the left semispan tip to allow movement of the ailavator. A schematic drawing of the glove is given in figure 1 and the ordinates used are presented in table I. The wing had no geometric twist or dihedral.

The wing was equipped with a 12.5-percent wing-root-chord trailing-edge plain ailavator having outboard and inboard segments of equal span capable of being deflected individually or in combination on the left semispan.

Photographs of the wing with the basic and round-nose configurations, mounted on the six-component balance system of the Langley full-scale tunnel, and close-up views of the ailavators, are given in figure 2.

TESTS

Tests were made on the sharp-leading-edge and round-nose configurations to determine lift, drag, rolling, yawing, and hinge moments at zero yaw through an angle-of-attack range from -5.2° to $+33.3^\circ$ for ailavator deflections in increments of 5° from -30° to $+30^\circ$. Hinge moments of each segment of the ailavators were measured for the segments deflected individually and for the segments deflected together in order to evaluate the interaction between them. No measurements were made of the hinge moments of the full semispan ailavator as a unit, but the sum of the hinge moments of the individual segments measured with the segments deflected together should be identically equal to the hinge moments of the unit.

For all tests the dynamic pressure was 7.3 pounds per square foot, resulting in a Reynolds number based on the mean aerodynamic chord of 6.00×10^6. The airspeed was approximately 55 miles per hour, corresponding to a Mach number of about 0.07.

The data were corrected for effects of jet-boundary interference, air-stream misalinement, buoyancy, and blocking. Support tare corrections were not investigated since they were found to be negligible in reference 5 for an identical wing and support setup.

RESULTS AND DISCUSSION

Presentation of Data

To facilitate discussion of the results, the presentation of data is outlined below.

The longitudinal characteristics including lift, drag, and pitching-moment coefficients of the basic and round-nose wings as affected by angle-of-attack change and outboard, inboard, and semispan ailavator deflections are shown in figures 3 to 10. Figures 6 and 10 are summary figures of the variations of C_m and C_L with δ_L at $\alpha = 0^\circ$, and $\left(C_{m_\delta}\right)_L$ and $\left(C_{L_\delta}\right)_L$ with α.

The lateral characteristics including rolling and yawing-moment coefficients for both wing configurations are shown in figure 11 and 12. Figure 13 is a summary figure of the variation of $\left(C_{n_\delta}\right)_L$ and $\left(C_{l_\delta}\right)_L$ with angle of attack.

The hinge-moment characteristics of each ailavator segment with the segments deflected individually or together are shown in figures 14 and 15. Figure 16 presents the variation of hinge moment with ailavator deflection for zero angle of attack, and figure 17 summarizes the variation of $\left(C_{h_\delta}\right)_L$ with angle of attack.

In some instances the ailavators were not set precisely at the desired angle and results for constant-deflection angles of the ailavators were interpolated from faired data curves.

Longitudinal Characteristics

Basic wing.- As discussed in detail in reference 3, the existence of a separation vortex, which is characteristic of highly swept wings having small leading-edge radii, has a tendency to increase the lift on outboard portions of the wing. As the angle of attack is increased, however, the vortex sweeps inboard towards the plane of symmetry, and, as a result, the outboard portion becomes completely stalled. As seen in figures 3(a) and 5(a), positive deflections of the outboard segment produced rather large increases in lift-curve slope and rearward shifts in center of pressure at lift coefficients from approximately 0.3 to 0.6. At lift coefficients just above 0.6, the outboard portions become completely stalled; hence, a decrease in lift-curve slope and an abrupt unstable change in pitching moment resulted. These changes were intensified with increased outboard ailavator deflections. With an increase in angle of attack the stall spreads farther over the inboard portions and the pitching-moment variation becomes stable for all flap deflections. As a result of this separation progression over the wing, the effectiveness $\left(C_{L_\delta}\right)_L$ of the outboard ailavator first increases and then decreases as the angle of attack is increased (see fig. 6).

The maximum C_L for the basic wing with ailavators undeflected was 1.08 and was reached at an angle of attack of 33.3°. As the ailavators were deflected to angles over 10°, the minimum drag began to increase appreciably and the variation of drag with lift became greater.

Effect of adding nose glove.- As shown in reference 2, rounding the sharp leading edge of a full-scale triangular wing to 0.0025c removed the force breaks with the flaps undeflected but not with the flaps deflected. Increasing the leading-edge radius to 0.011c had no further significant effect. In the present tests, installing the NACA 65-010 nose glove with a leading-edge radius of 0.00687c resulted in removing all irregularities in the lift-curve slopes and unstable breaks in the pitching moments (figs. 7 to 9).

As a result of the absence of the vortex flow, the irregularities in the variation of $\left(C_{L_\delta}\right)_L$ and $\left(C_{m_\delta}\right)_L$ with angle of attack, which were observed in the sharp-leading-edge configuration (fig. 6), were removed by changing to the NACA 65-010 leading edge (fig. 10). With the nose glove installed, the outboard ailavator shows a gradual decrease in both lift and moment effectiveness and the inboard ailavator shows practically no change as the angle of attack was increased. It is of interest also to note that at all but the lowest angles of attack the flap effectiveness is appreciably greater for the basic wing than for the round-nose wing; possibly positive flap deflection at a fixed angle of attack tends to increase the size of the vortex and provide, thereby, an additional lift increment.

For a given high-lift coefficient positive ailavator deflections produced smaller C_D values than negative deflections for all ailavator configurations tested. For a positive deflection of 30°, the inboard ailavator generally produced the least drag.

From data obtained but not presented, it was found that sealing the gap at the ailavator leading edge with the ailavator at zero deflection had a negligible effect on the longitudinal characteristics of the wing.

Lateral Characteristics

Basic wing.- For moderate ailavator deflections, the variation of rolling moment with deflection, as shown in figure 11, was fairly linear at every angle of attack. As would be expected, the semispan ailavator produced the greater rolling moment.

The point for which the lift coefficient is 85 percent of $C_{L_{max}}$, which is considered representative of the usable C_L for the landing condition, is indicated on the ailavator-effectiveness parameter $\left(C_{l_\delta}\right)_L$ curve in figure 13(a). For the outboard, inboard, and semispan ailavators, the values of $\left(C_{l_\delta}\right)_L$ at $0.85C_{L_{max}}$ are 0.00065, 0.00065, and 0.0014, respectively. After the loss of additional lift at the tips, caused by the inboard displacement of the conical vortex, the outboard and semispan ailavators lost effectiveness with increasing angles of attack. The outboard-ailavator effectiveness at $0.85C_{L_{max}}$ was one-half that measured at an angle of attack of approximately 10°, just prior to wing-tip stall. The rolling effectiveness of the semispan ailavator is very nearly the sum of the effectivenesses of the two segments over the lift-coefficient range.

Favorable yawing moments were produced by negative deflections of the ailavators at angles of attack up to 5.3°, but with angles of attack

over 5.3°, there was an adverse yawing moment produced (fig. 11(b)). Positive deflections of the ailavators produced adverse yawing moments for the entire range of α. The value of $\left(C_{n_\delta}\right)_L$ becomes more negative with increasing values of α, the variation being nearly linear for the basic wing as shown in figure 13(a).

Effect of adding nose glove.- For the round-nose configuration the variation of rolling moment with ailavator deflection was fairly linear at each angle of attack except near stall, as shown in figure 12(a), but the values of C_l were not as large as those for the basic wing. The inboard ailavator produced values of $\left(C_{l_\delta}\right)_L$ about one-third and the outboard ailavator about two-thirds those of the full semispan ailavator at low and moderate angles of attack as shown in figure 13(b). At high angles of attack, however, the outboard-ailavator effectiveness decreased rapidly such that the values of $\left(C_{l_\delta}\right)_L$ at $0.85C_{L_{max}}$ were 0.00050, 0.00055, and 0.00115 for outboard, inboard, and semispan ailavators, respectively.

The round-nose configuration displayed the favorable yawing moments noted on the basic wing for negative ailavator deflections at angles of attack up to 10.7° (fig. 12(b)). At greater angles of attack negative ailavator deflections produced adverse moments. Positive deflections of the ailavators produced adverse yawing moments for the entire range of α.

Hinge-Moment Characteristics

Basic and round-nose wings.- The development of the characteristic type of vortex flow resulting from leading-edge separation on the sharp-leading-edge wing introduced severe hinge-moment discontinuities with large ailavator deflections (fig. 14). The round-nose wing has smooth hinge-moment characteristics throughout the lift-coefficient range except with high negative ailavator deflections (fig. 15).

For both wings, the inboard ailavator values of $\left(C_{h_\delta}\right)_L$ at low and moderate angles of attack (figs. 16 and 17) were zero or very small for small deflections. For larger angles of attack and high positive or negative ailavator deflection angles, values of $\left(C_{h_\delta}\right)_L$ attained the usual high negative values. Hinge-moment characteristics of this type are fairly common for controls having large trailing-edge angles.

(See reference 6.) Comparison of data for ailavators deflected individually and together with the other segment shows very little interaction.

SUMMARY OF RESULTS

The significant results of the investigation at low speed of the effectiveness and hinge-moments of a constant-chord ailavator on a large-scale triangular wing with symmetrical biconvex sections and also with the sections modified by installing an NACA 65-010 nose glove are summarized as follows:

1. The characteristic force breaks caused by a separation vortex on the basic sharp-edged airfoil were eliminated by installing the NACA 65-010 nose glove.

2. For the basic wing, the values for the ailavator-effectiveness parameter $\left(C_{l_\delta}\right)_L$ for the outboard, inboard, and semispan ailavators at $0.85C_{L_{max}}$ were 0.00065, 0.00065, and 0.0014; for the round-nose wing the values were 0.00050, 0.00055, and 0.00115, respectively.

3. The effectiveness and hinge moments of the full semispan ailavator for both wings represent the sum of the characteristics of the two segments.

4. The leading-edge separation vortex on the sharp-edged wing introduced large hinge-moment discontinuities with large ailavator deflections.

Langley Aeronautical Laboratory
National Advisory Committee for Aeronautics
Langley Field, Va.

REFERENCES

1. Wilson, Herbert A., Jr., and Lovell, J. Calvin: Full-Scale Investigation of the Maximum Lift and Flow Characteristics of an Airplane Having Approximately Triangular Plan Form. NACA RM L6K20, 1946.

2. Anderson, Adrien E.: An Investigation at Low Speed of a Large-Scale Triangular Wing of Aspect Ratio Two. II. The Effect of Airfoil Section Modifications and the Determination of the Wake Downwash. NACA RM A7H28, 1947.

3. May, Ralph W., Jr., and Hawes, John G.: Low-Speed Pressure-Distribution and Flow Investigation for a Large Pitch and Yaw Range of Three Low-Aspect-Ratio Pointed Wings Having Leading Edge Swept Back 60° and Biconvex Sections. NACA RM L9J07, 1949.

4. Orlik-Rückeman, K.: Experimental Determination of Pressure Distributions and Transition Lines of Plane Delta Wings at Low Speeds and Zero Yaw. KTH - Aero TN 3, Roy. Inst. of Technology, Div. of Aero., Stockholm, Sweden, 1948.

5. Whittle, Edward F., Jr., and Lovell, J. Calvin: Full-Scale Investigation of an Equilateral Triangular Wing Having 10-Percent-Thick Biconvex Airfoil Sections. NACA RM L8G05, 1948.

6. Langley Research Staff (Compiled by Thomas A. Toll) Summary of Lateral-Control Research. NACA Rep. 868, 1947.

TABLE I.- AIRFOIL ORDINATES PARALLEL TO PLANE OF SYMMETRY OF WING CONFIGURATIONS TESTED

[All dimensions in percent chord]

Station	Ordinate	
	Basic wing (10-percent-thick biconvex)	Wing with NACA 65-010 glove
0	--------	----------
.50	--------	0.77
.75	--------	.93
1.25	0.25	1.17
2.5	.49	1.57
5.0	.96	2.18
7.5	1.40	2.65
10	1.81	3.04
15	2.56	3.66
20	3.21	4.07
25	3.75	4.42
30	4.21	4.67
35	4.55	4.81
40	4.80	4.92
45	4.95	4.98
50	5.00	5.00
55	4.95	4.95
60	4.80	4.80
65	4.55	4.55
70	4.21	4.21
75	3.75	3.75
80	3.21	3.21
85	2.56	2.56
90	1.81	1.81
95	.96	.96
100	--------	----------
		L.E. radius = 0.00687c

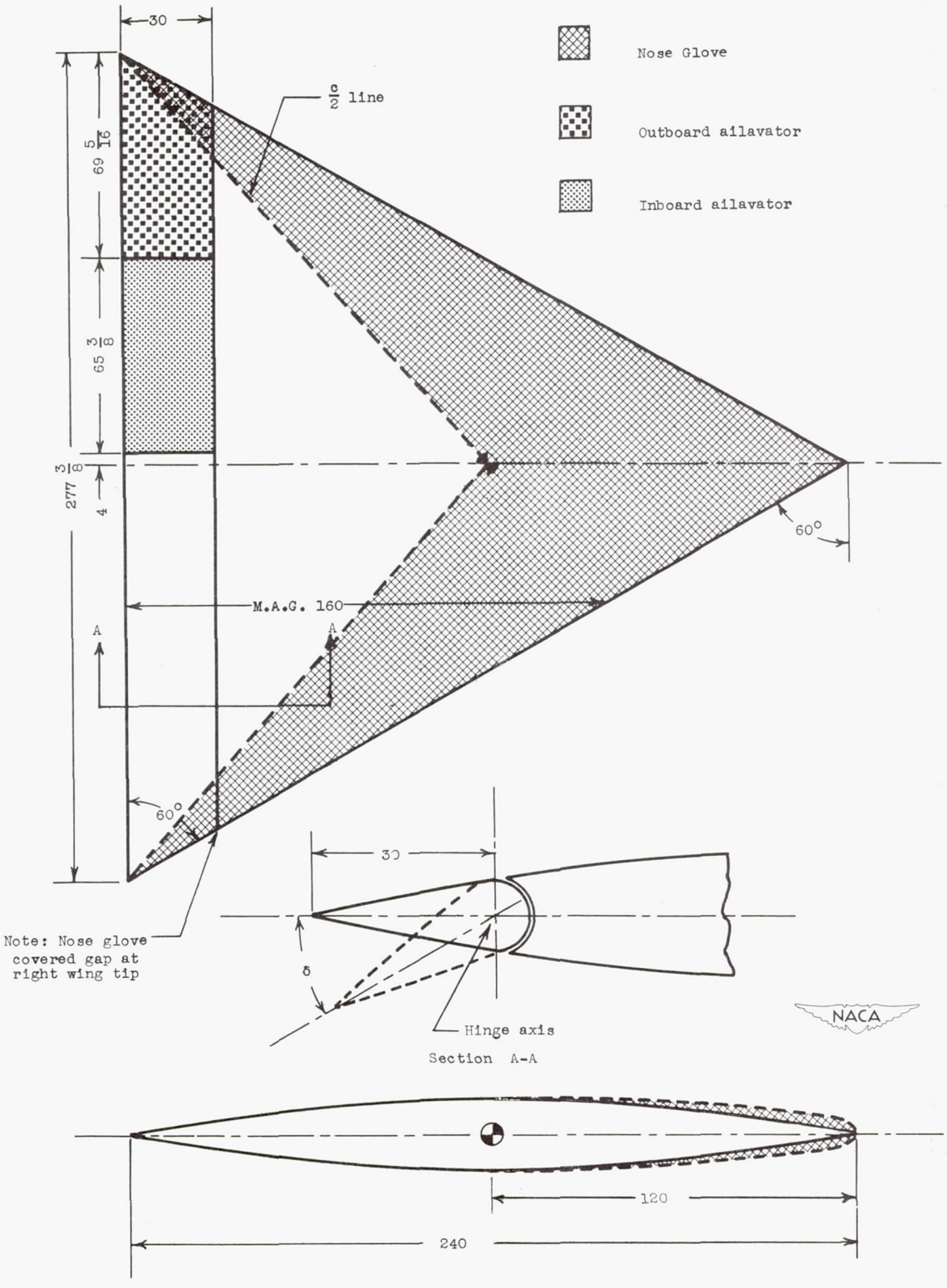

Figure 1.- Geometric characteristics of wing tested with and without an NACA 65-010 nose glove. All dimensions are in inches.

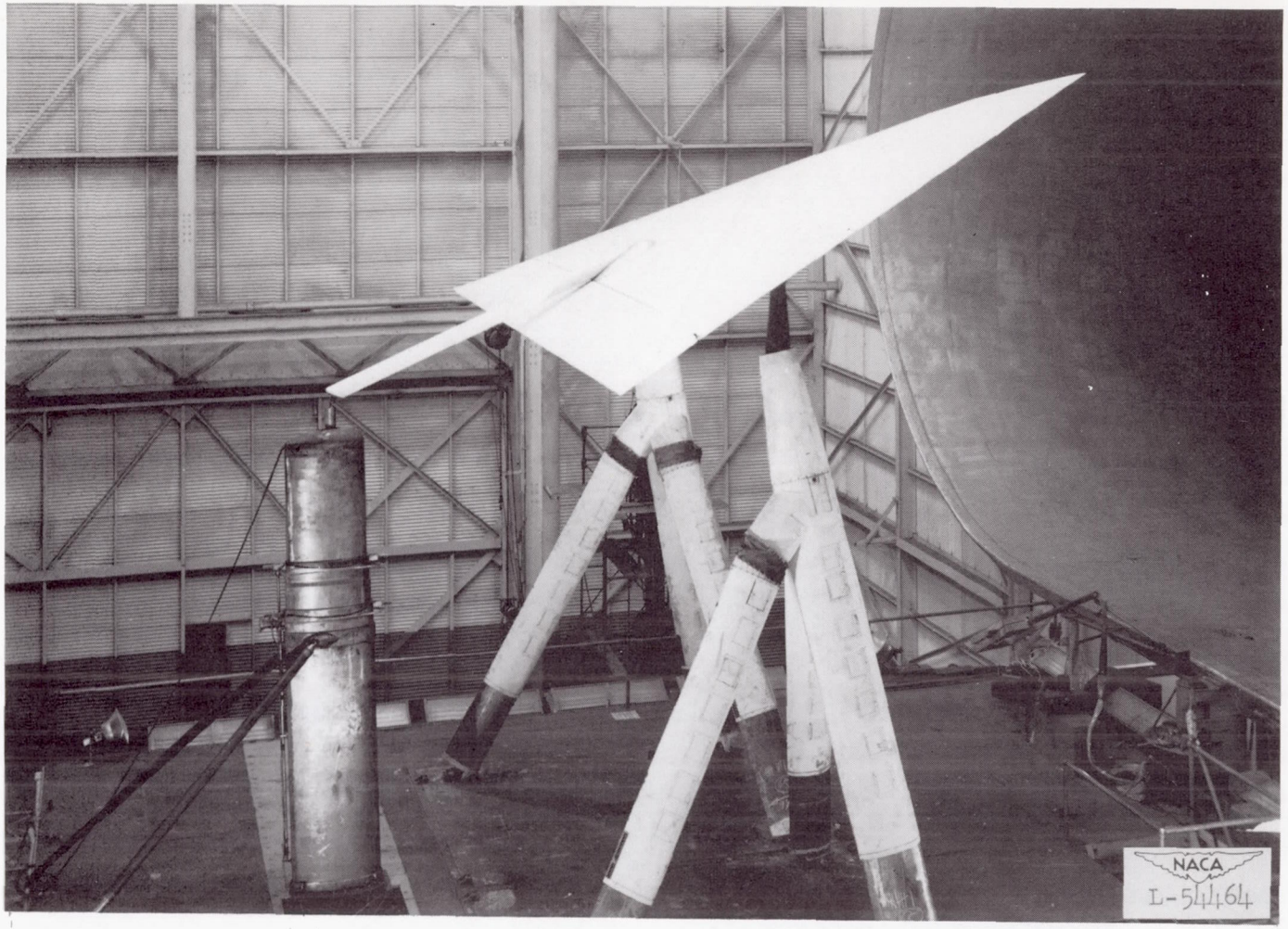

(a) Basic sharp-edged wing configuration.

Figure 2.- The low-aspect-ratio triangular wing mounted in the Langley full-scale tunnel.

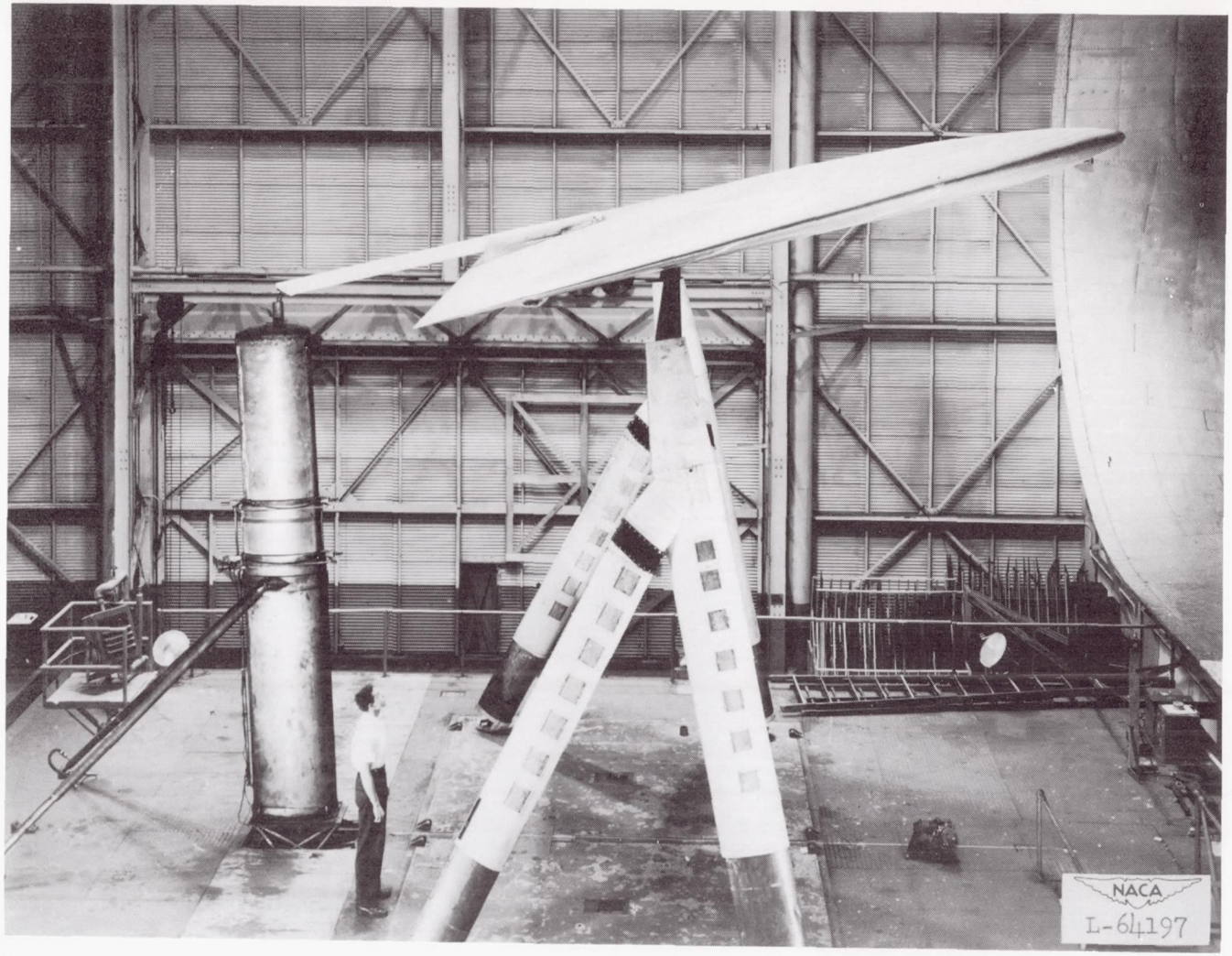

(b) NACA 65-010 round-nose glove configuration.

Figure 2.- Continued.

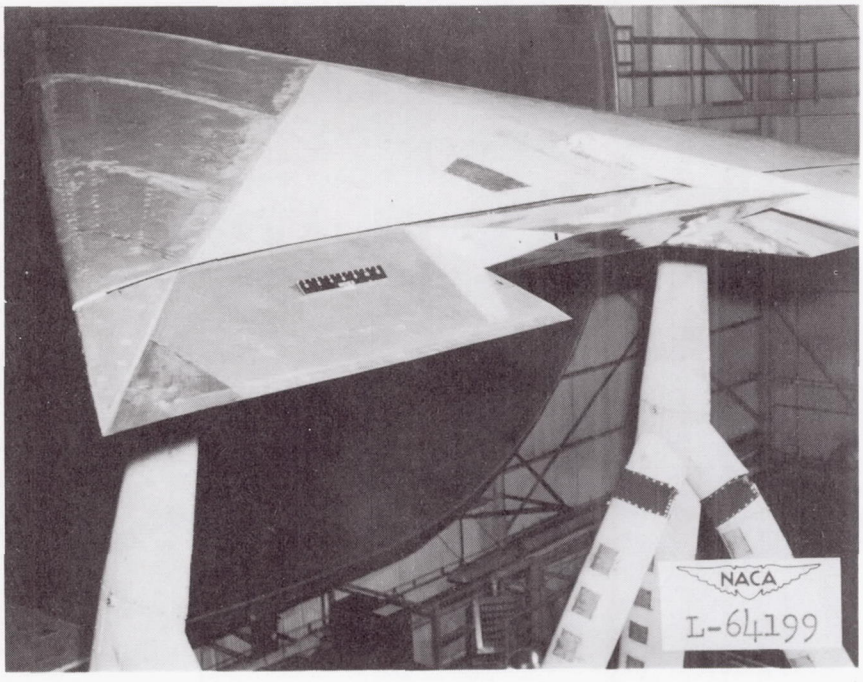

(c) Inboard left ailavator deflected upward.

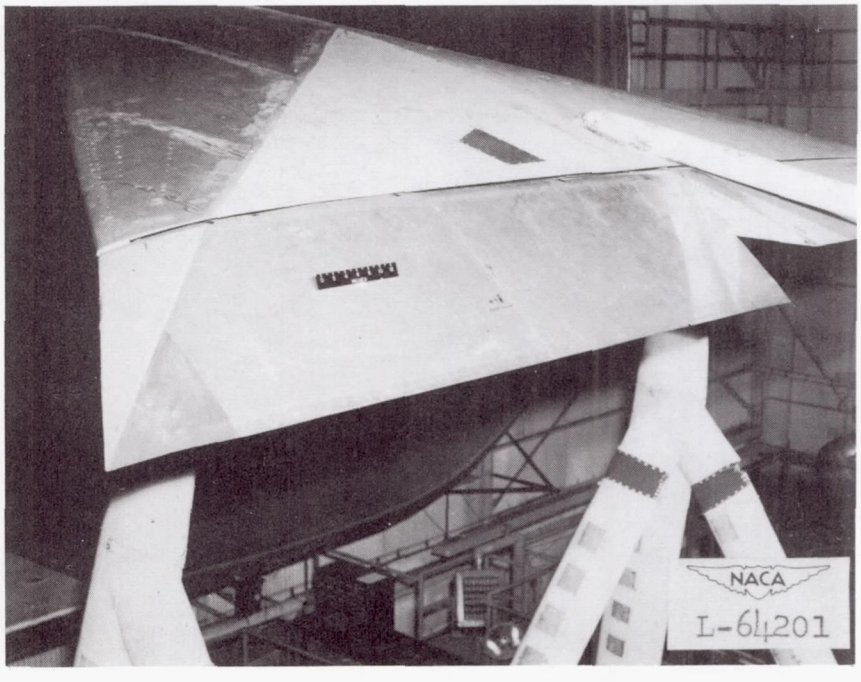

(d) Combination inboard and outboard left semispan ailavator deflected downward.

Figure 2.- Concluded.

(a) Variation of α and C_m with C_L.

Figure 3.- Effect of left outboard ailavator deflection on the longitudinal characteristics of the basic wing configuration.

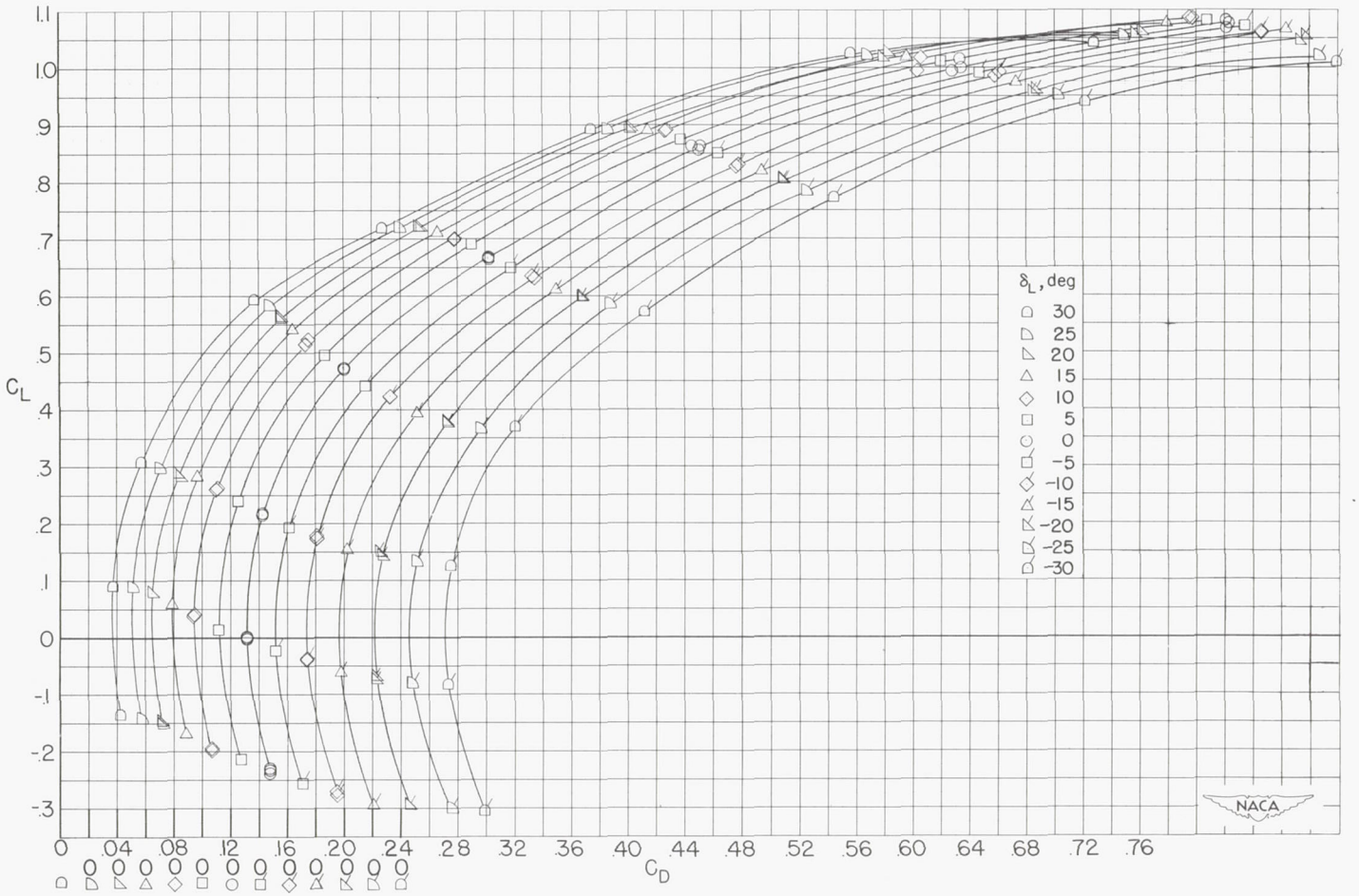

(b) Variation of C_D with C_L.

Figure 3.- Concluded.

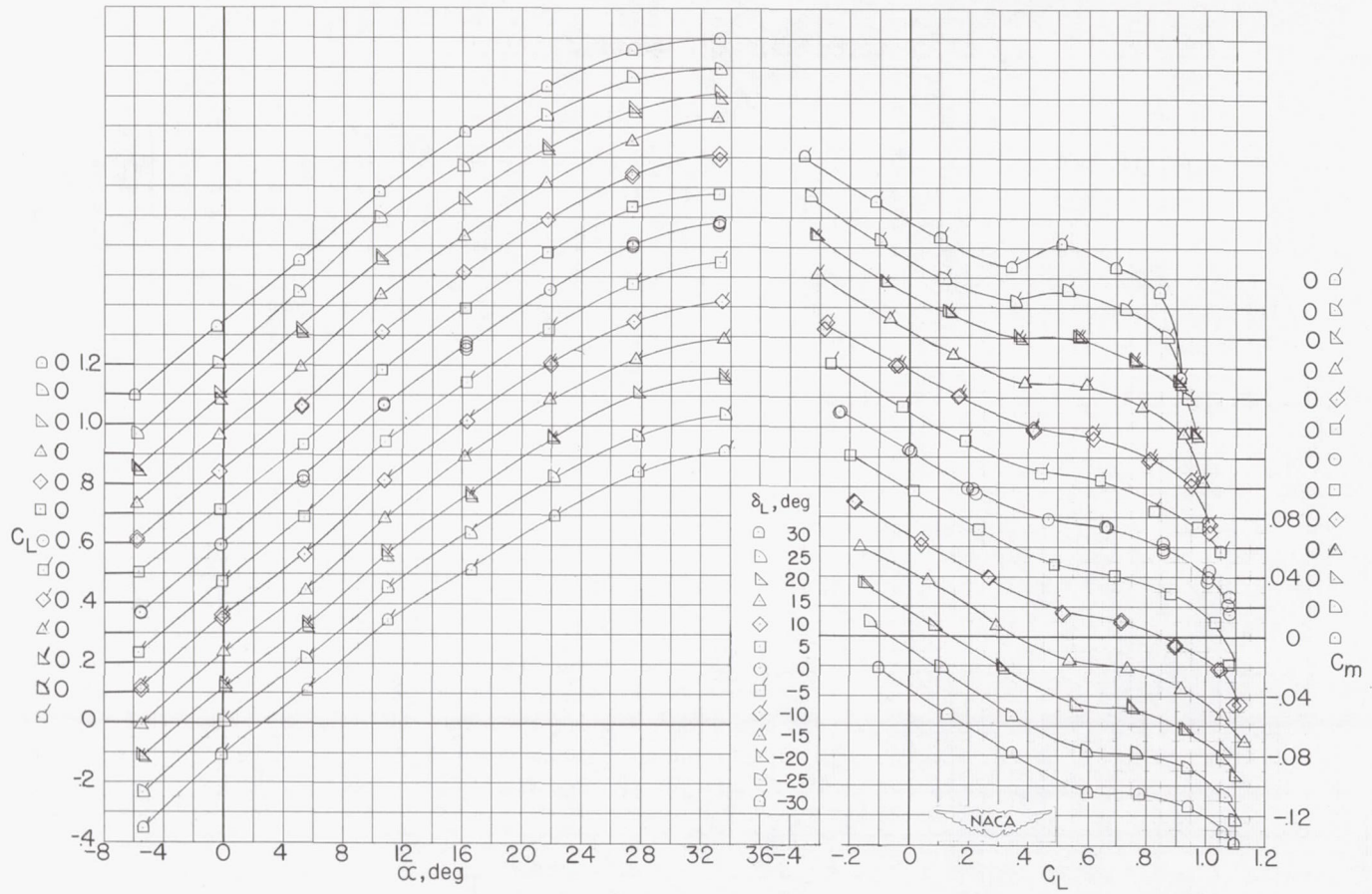

(a) Variation of α and C_m with C_L.

Figure 4.- Effect of left inboard ailavator deflection on the longitudinal characteristics of the basic wing configuration.

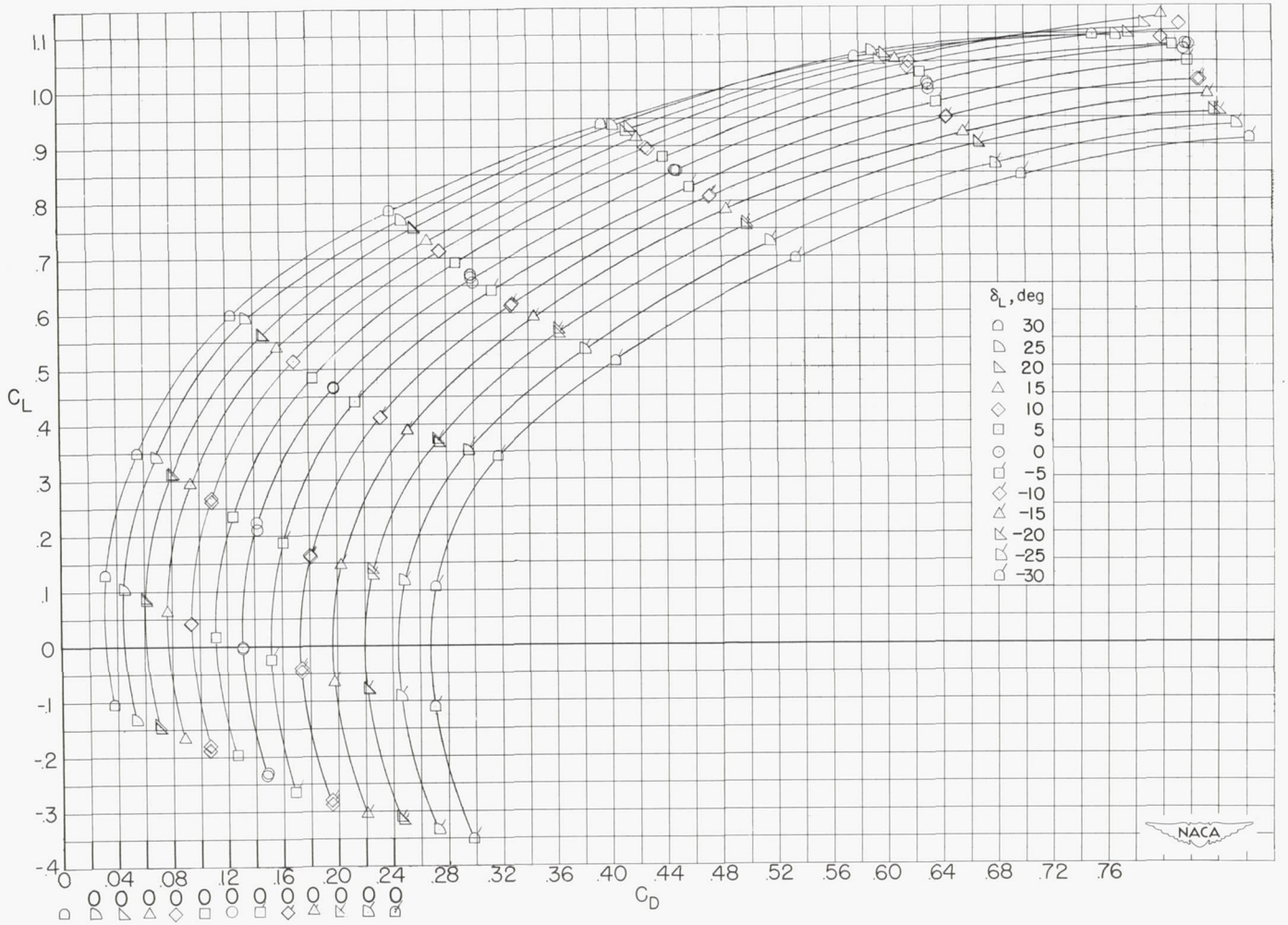

(b) Variation of C_D with C_L.

Figure 4.- Concluded.

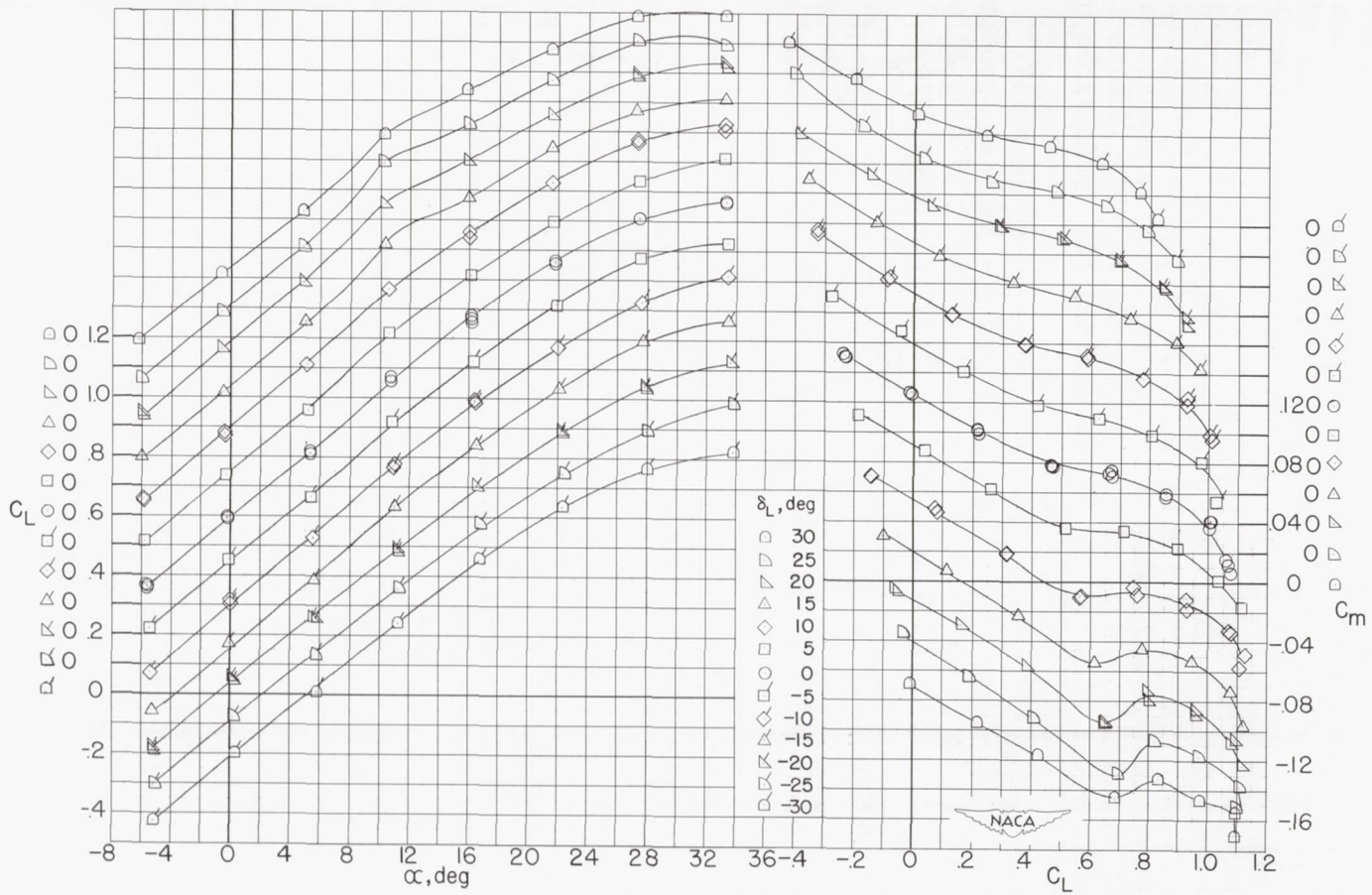

(a) Variation of α and C_m with C_L.

Figure 5.- Effect of left semispan ailavator deflection on the longitudinal characteristics of the basic wing configuration.

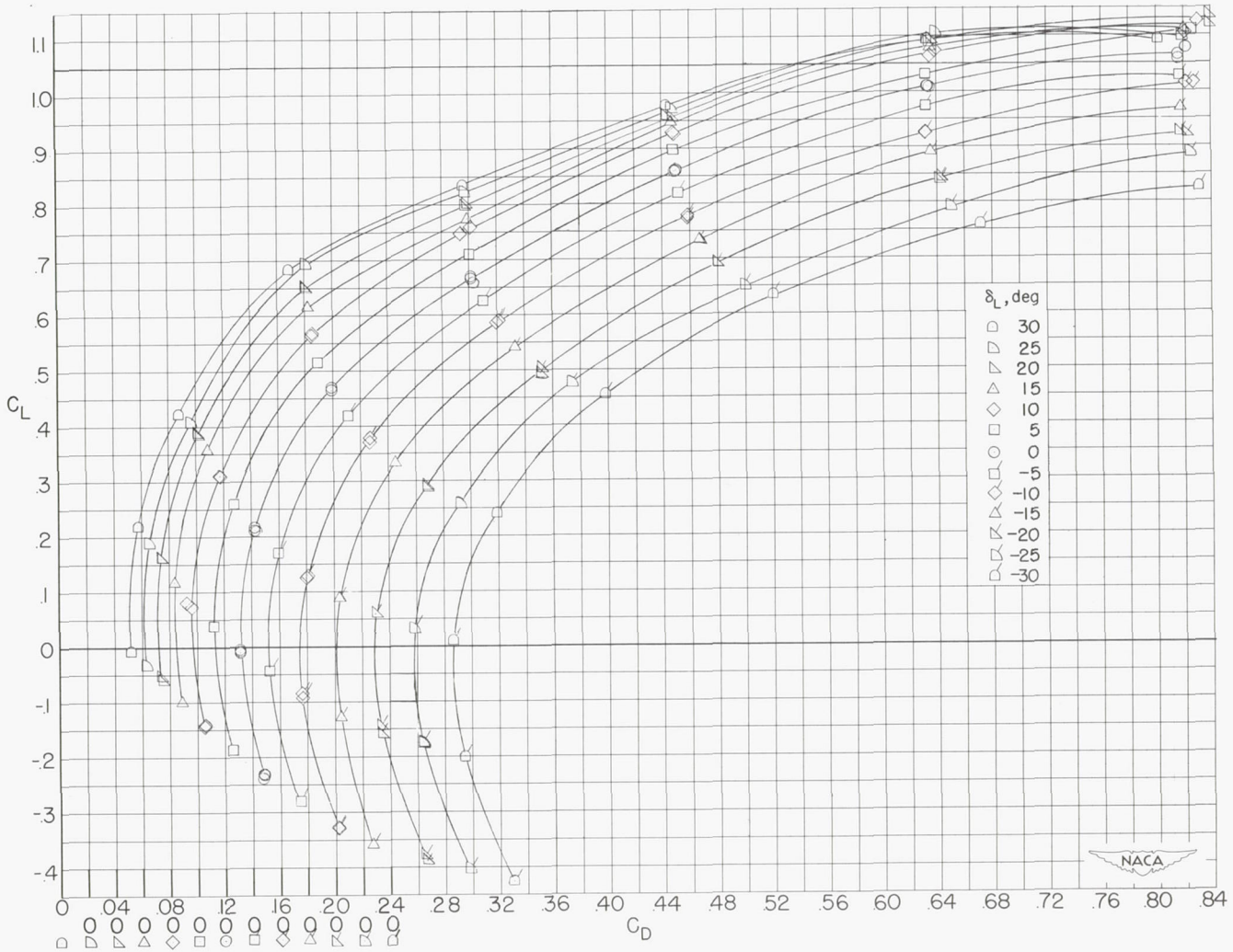

(b) Variation of C_D with C_L.

Figure 5.- Concluded.

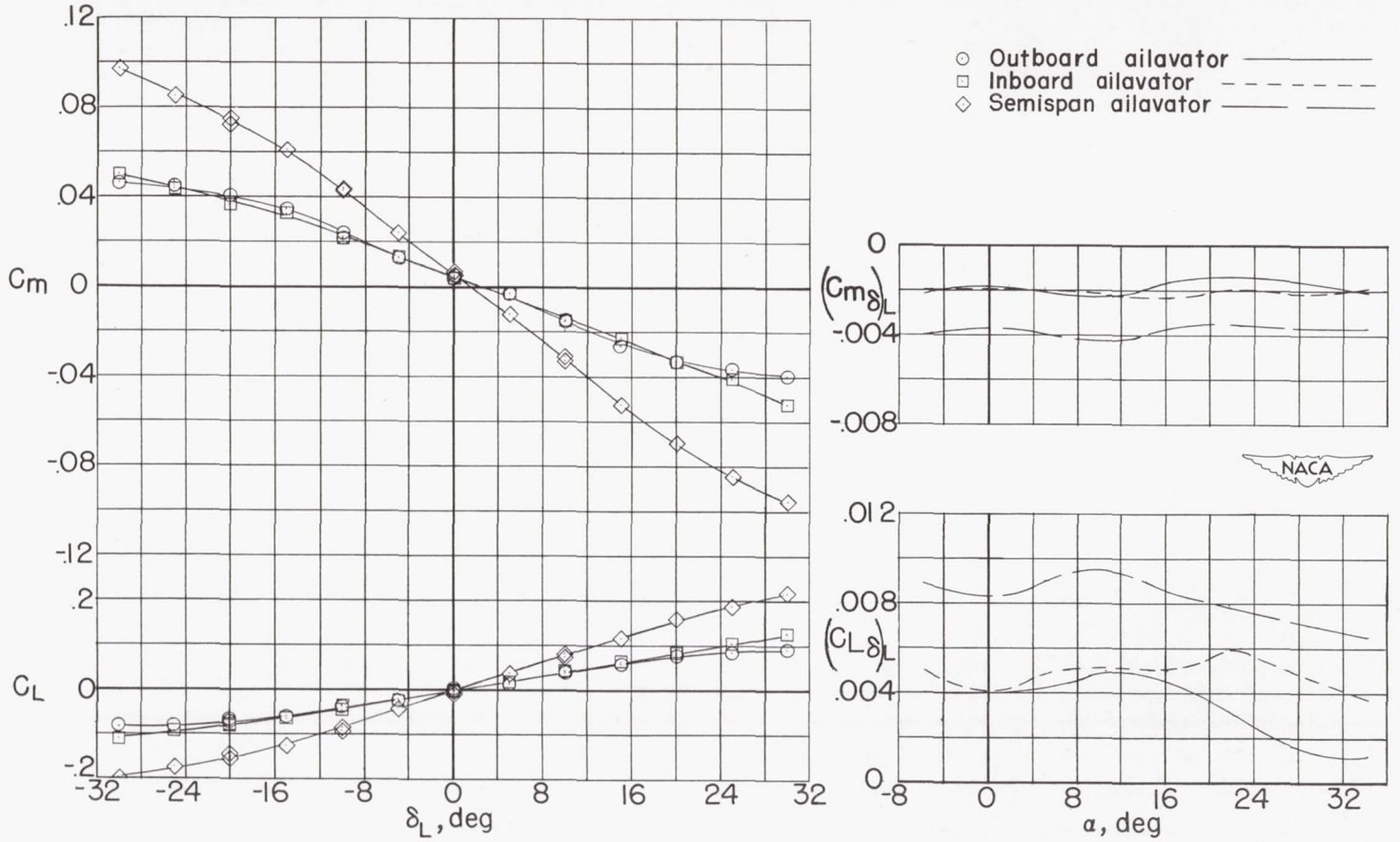

(a) Variation of C_m and C_L with δ_L. (b) Variation of $C_{m_{\delta_L}}$ and $C_{L_{\delta_L}}$ with α.

Figure 6.- Effect of left ailavator plan form on the variation of C_m and C_L with δ_L for zero uncorrected angle of attack and the variation of $C_{m_{\delta_L}}$ and $C_{L_{\delta_L}}$ with α for the basic wing configuration.

(a) Variation of α and C_m with C_L.

Figure 7.- Effect of left outboard ailavator deflection on the longitudinal characteristics of the round-nose wing configuration.

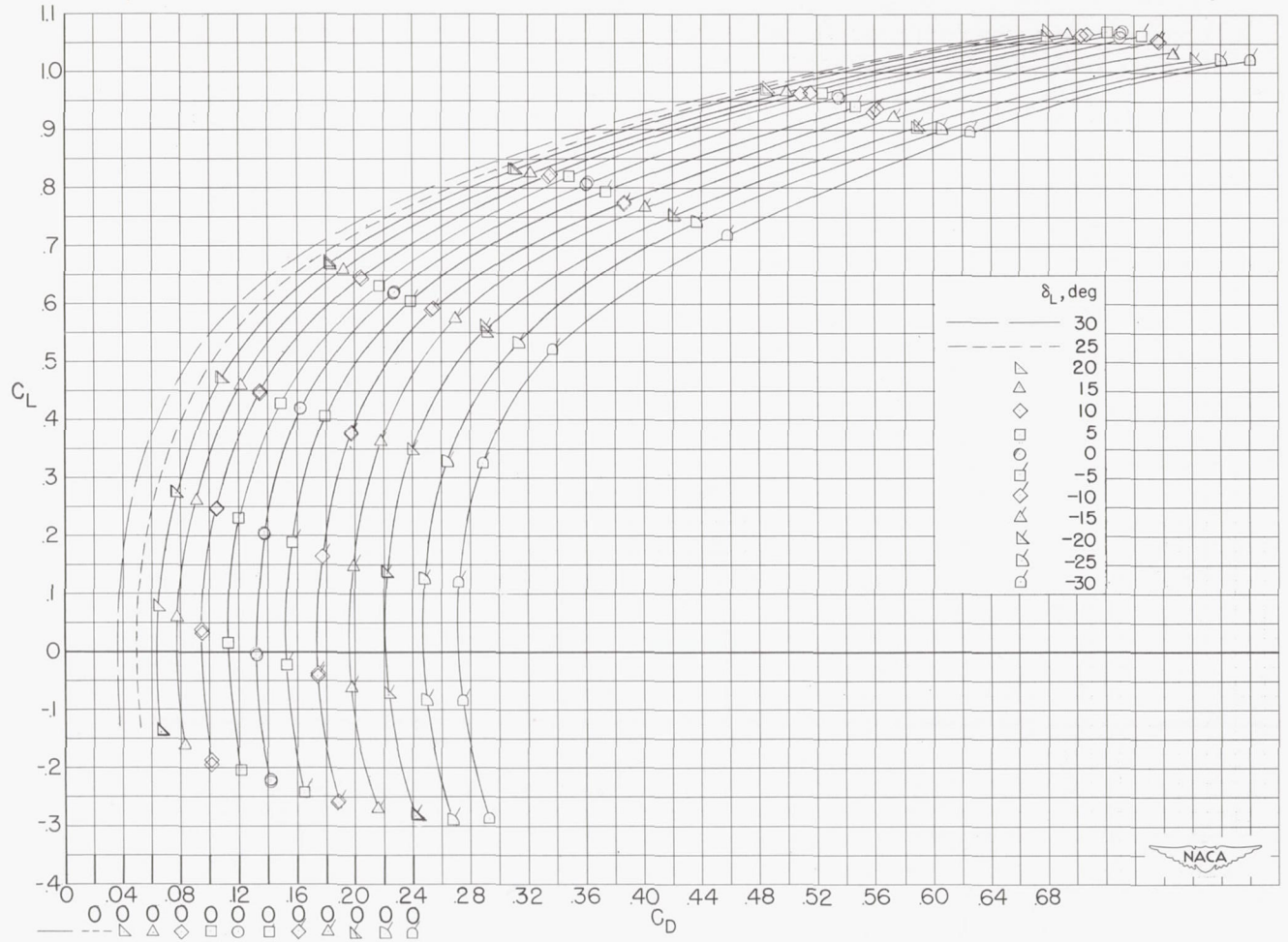

(b) Variation of C_D with C_L.

Figure 7.- Concluded.

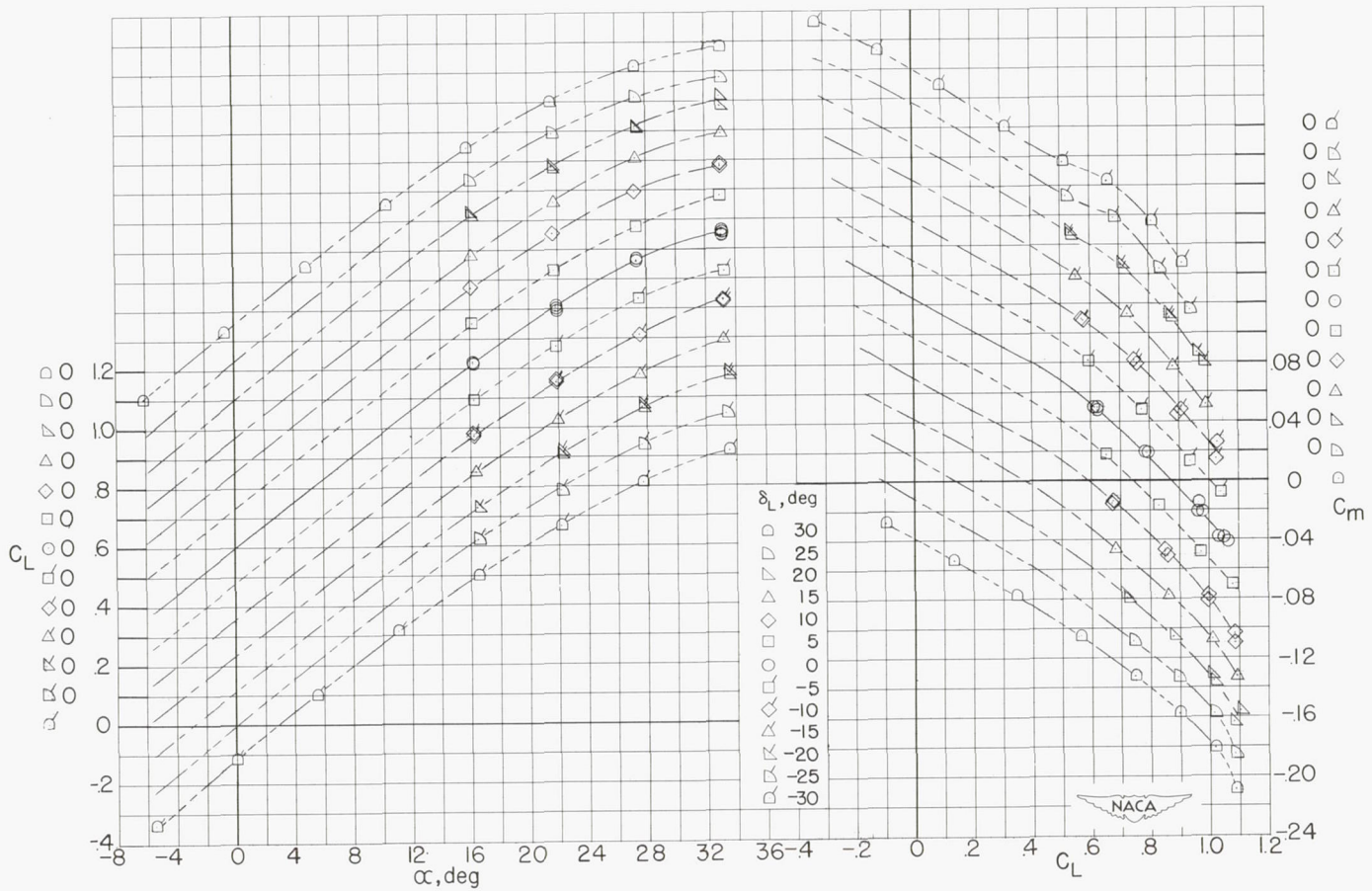

(a) Variation of α and C_m with C_L.

Figure 8.- Effect of left inboard ailavator deflection on the longitudinal characteristics of the round-nose wing configuration.

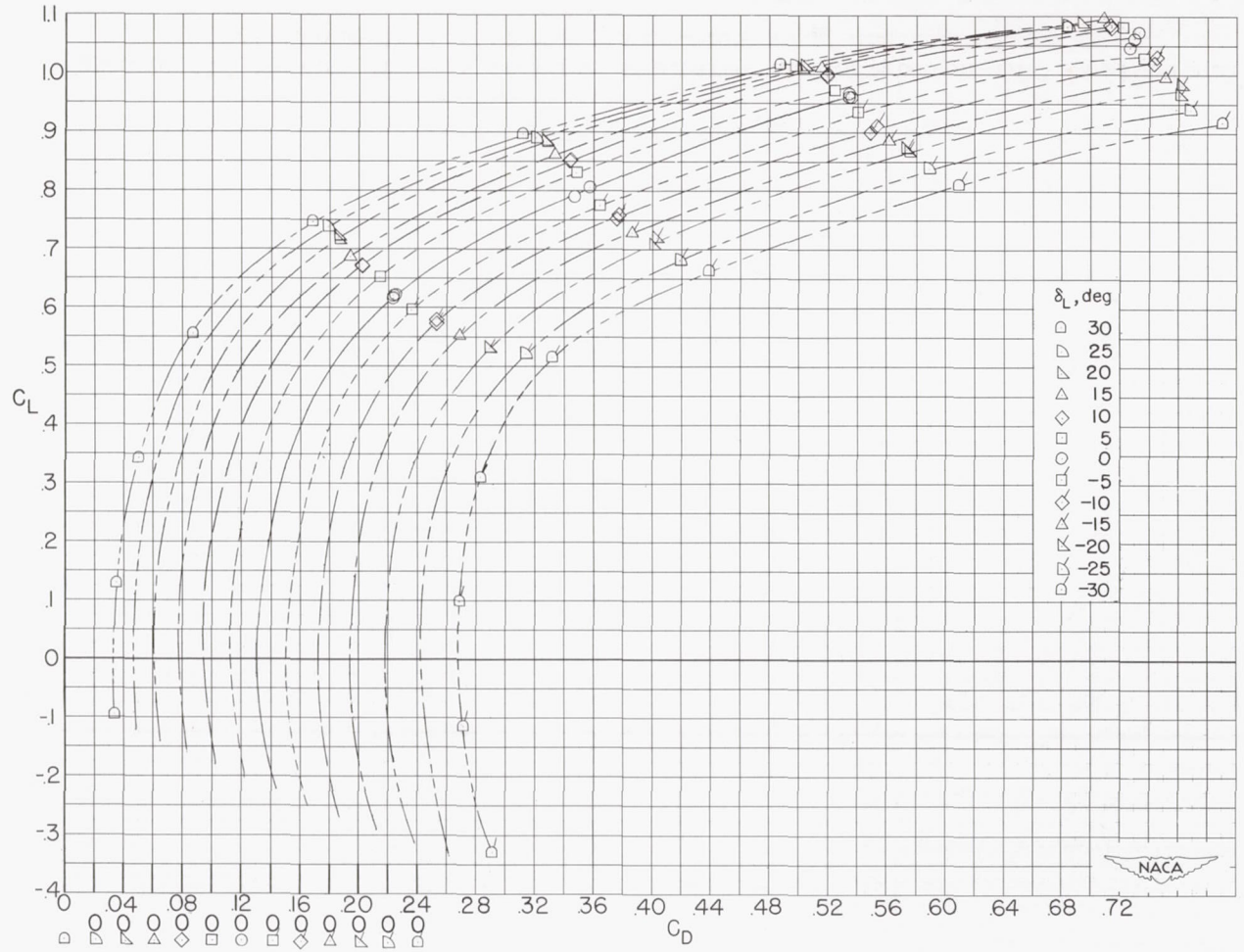

(b) Variation of C_D with C_L.

Figure 8.- Concluded.

(a) Variation of α and C_m with C_L.

Figure 9.- Effect of left semispan ailavator deflection on the longitudinal characteristics of the round-nose wing configuration.

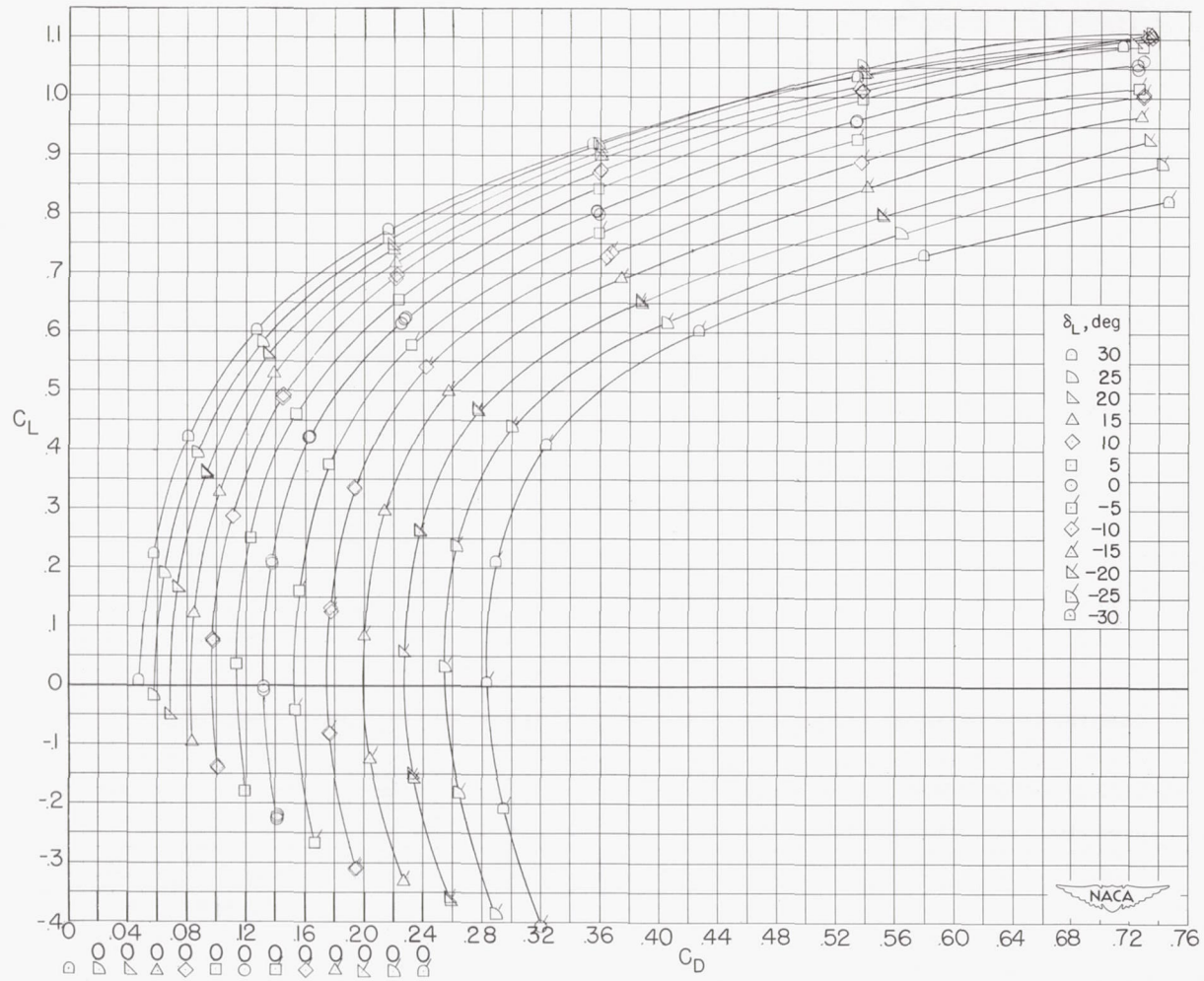

(b) Variation of C_D with C_L.

Figure 9.- Concluded.

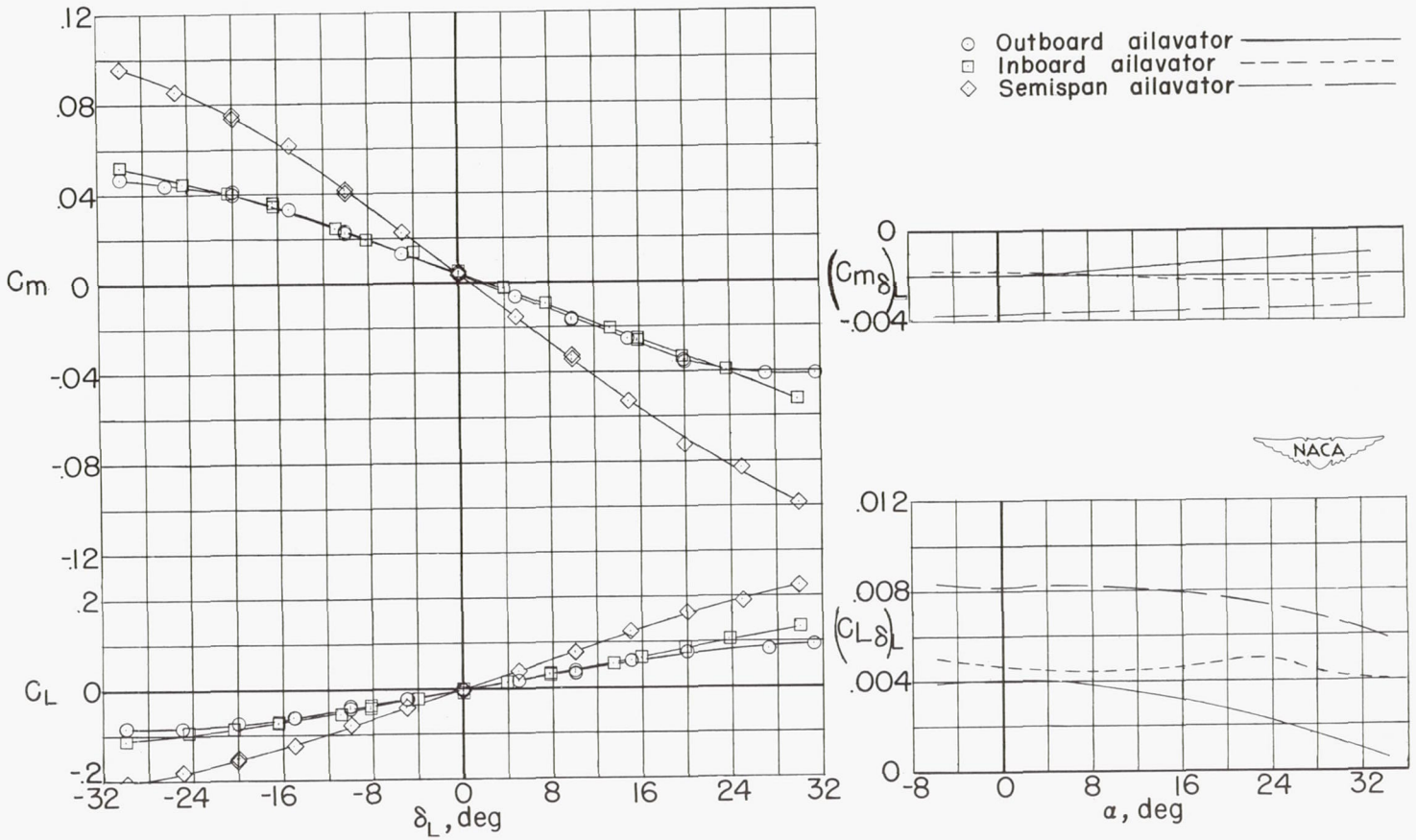

(a) Variation of C_m and C_L with δ_L. (b) Variation of $C_{m_{\delta_L}}$ and $C_{L_{\delta_L}}$ with α.

Figure 10.- Effect of left ailavator plan form on the variation of C_m and C_L with δ_L for zero uncorrected angle of attack and the variation of $C_{m_{\delta_L}}$ and $C_{L_{\delta_L}}$ with α for the round-nose wing configuration.

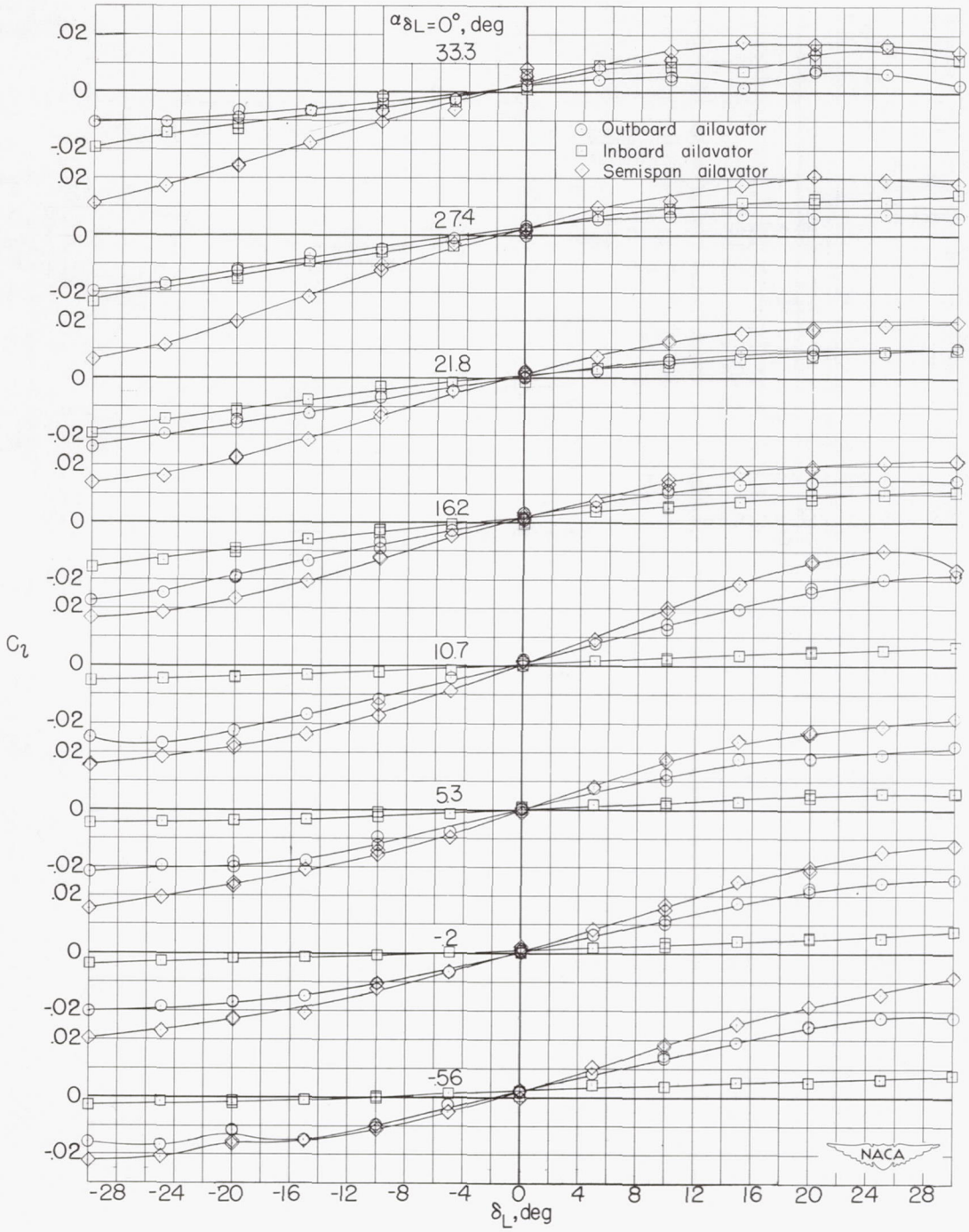

(a) Variation of C_l with δ_L.

Figure 11.- Effect of left ailavator deflection on the rolling- and yawing-moment characteristics of the basic wing configuration.

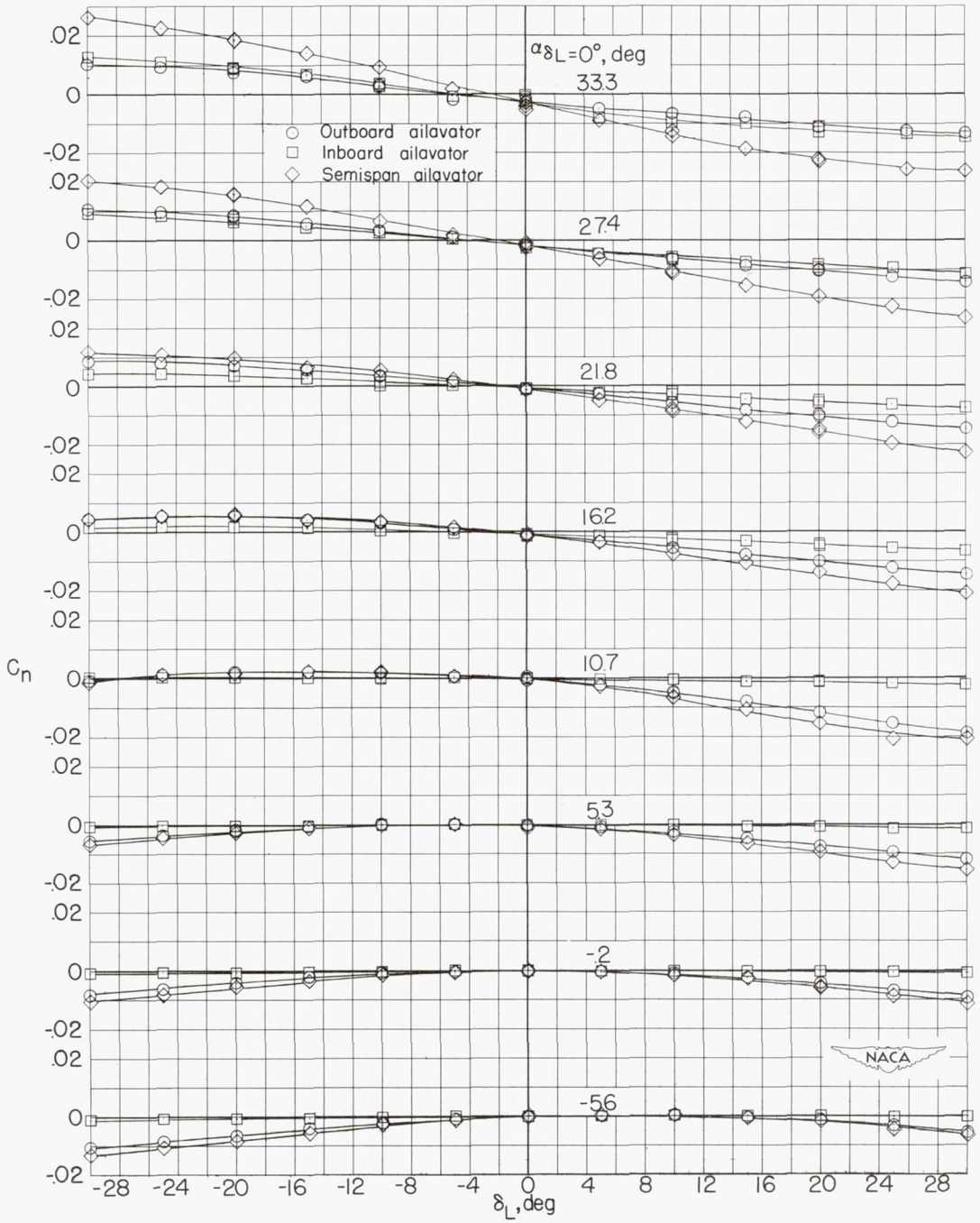

(b) Variation of C_n with δ_L.

Figure 11.- Concluded.

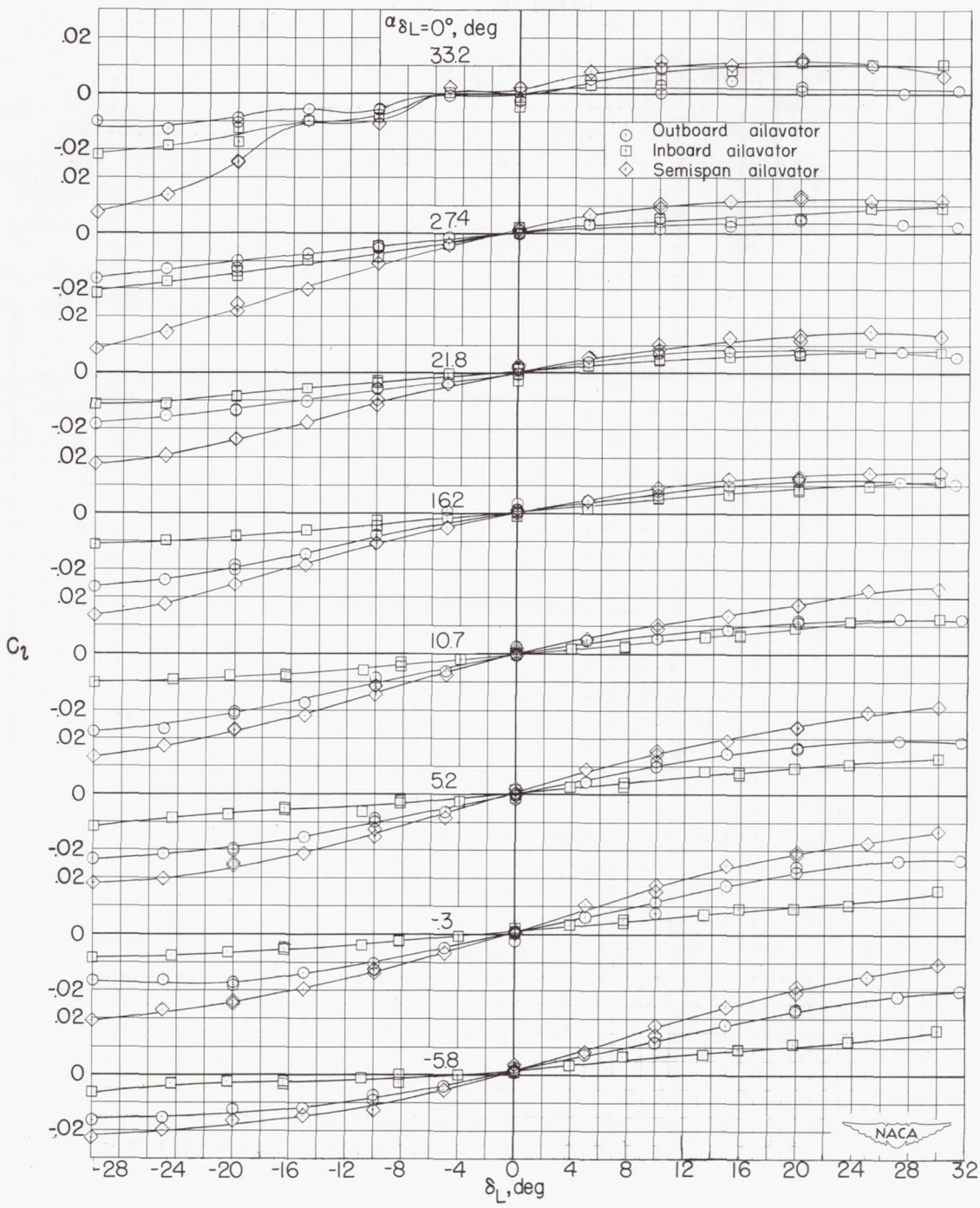

(a) Variation of C_l with δ_L.

Figure 12.- Effect of left ailavator deflection on the rolling- and yawing-moment characteristics of the round-nose wing configuration.

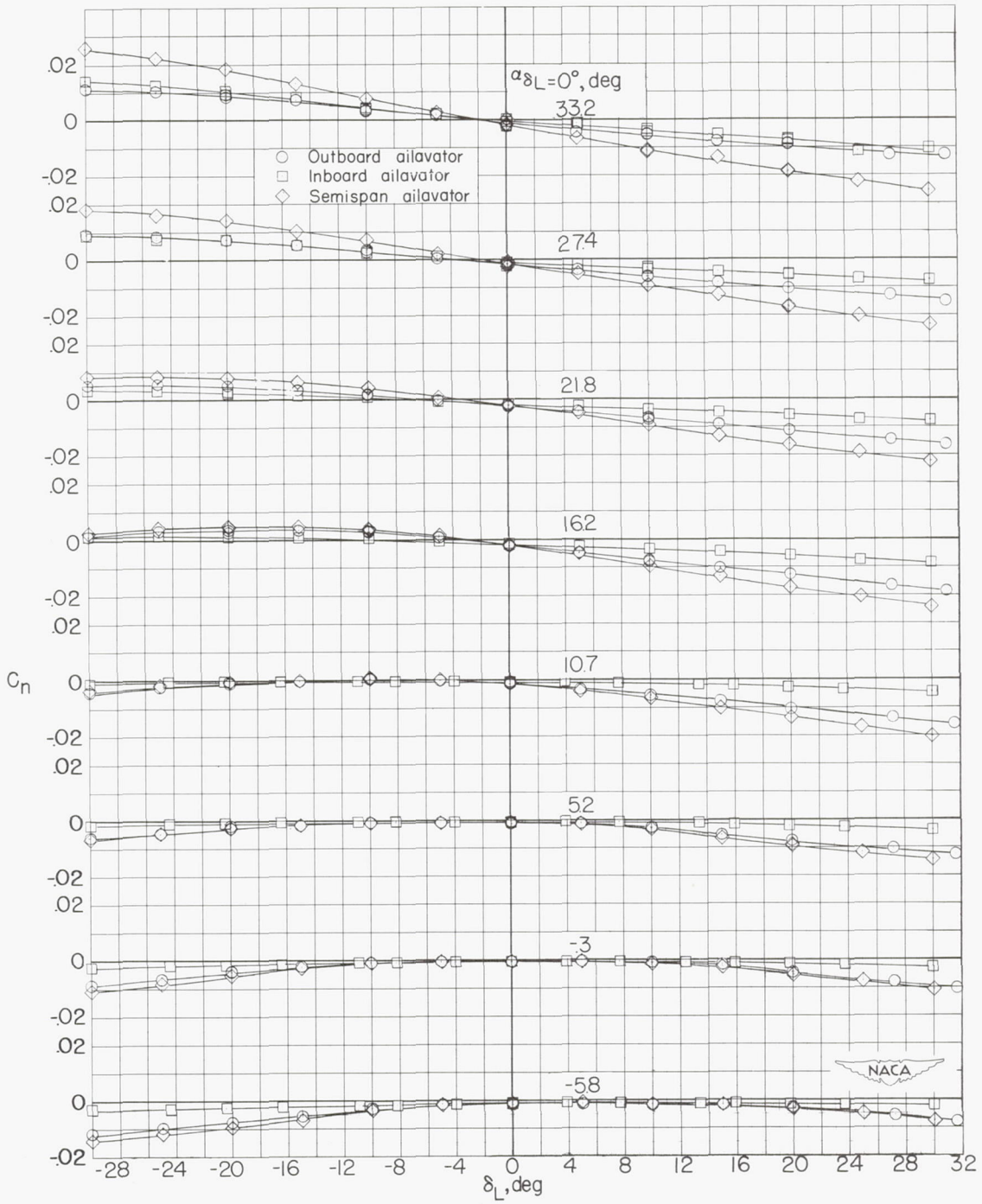

(b) Variation of C_n with δ_L.

Figure 12.- Concluded.

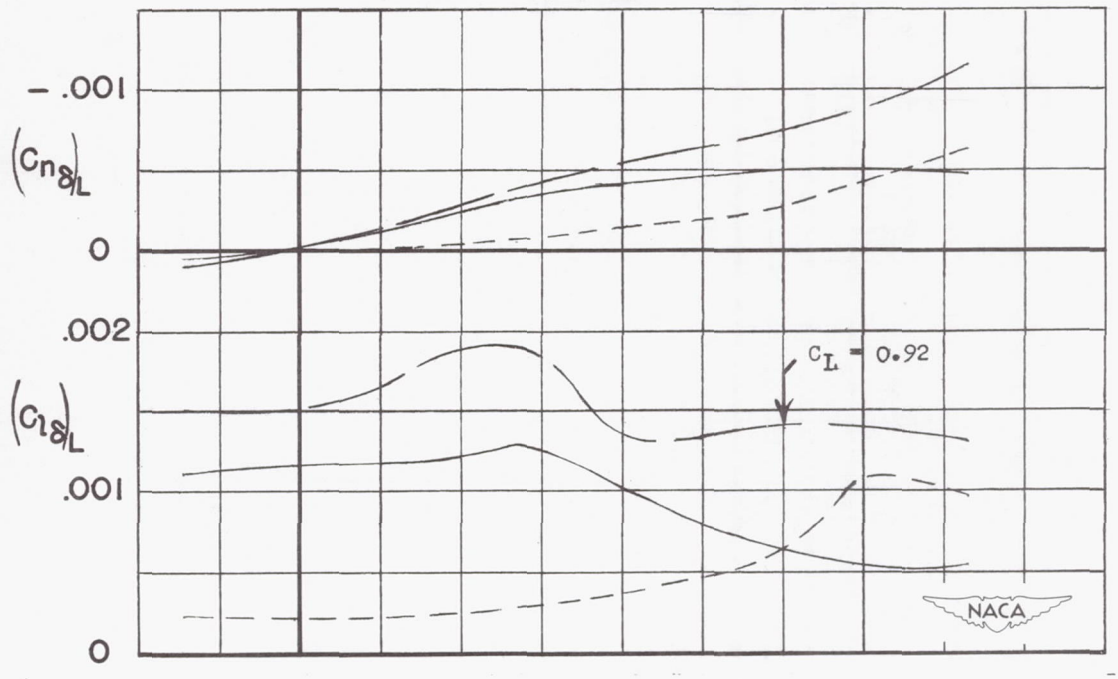

(a) Basic wing configuration.

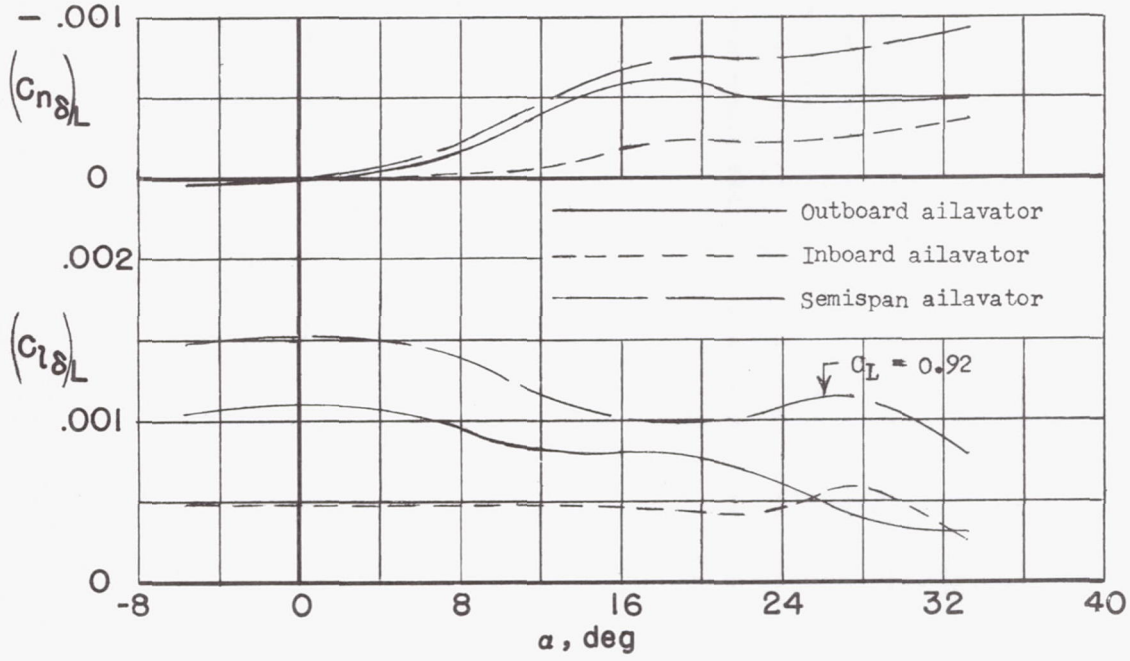

(b) Round-nose configuration.

Figure 13.- Variation of $(C_{n_\delta})_L$ and $(C_{l_\delta})_L$ with α. ($(C_{n_\delta})_L$ and $(C_{l_\delta})_L$ measured at $\delta_L = 0^\circ$.)

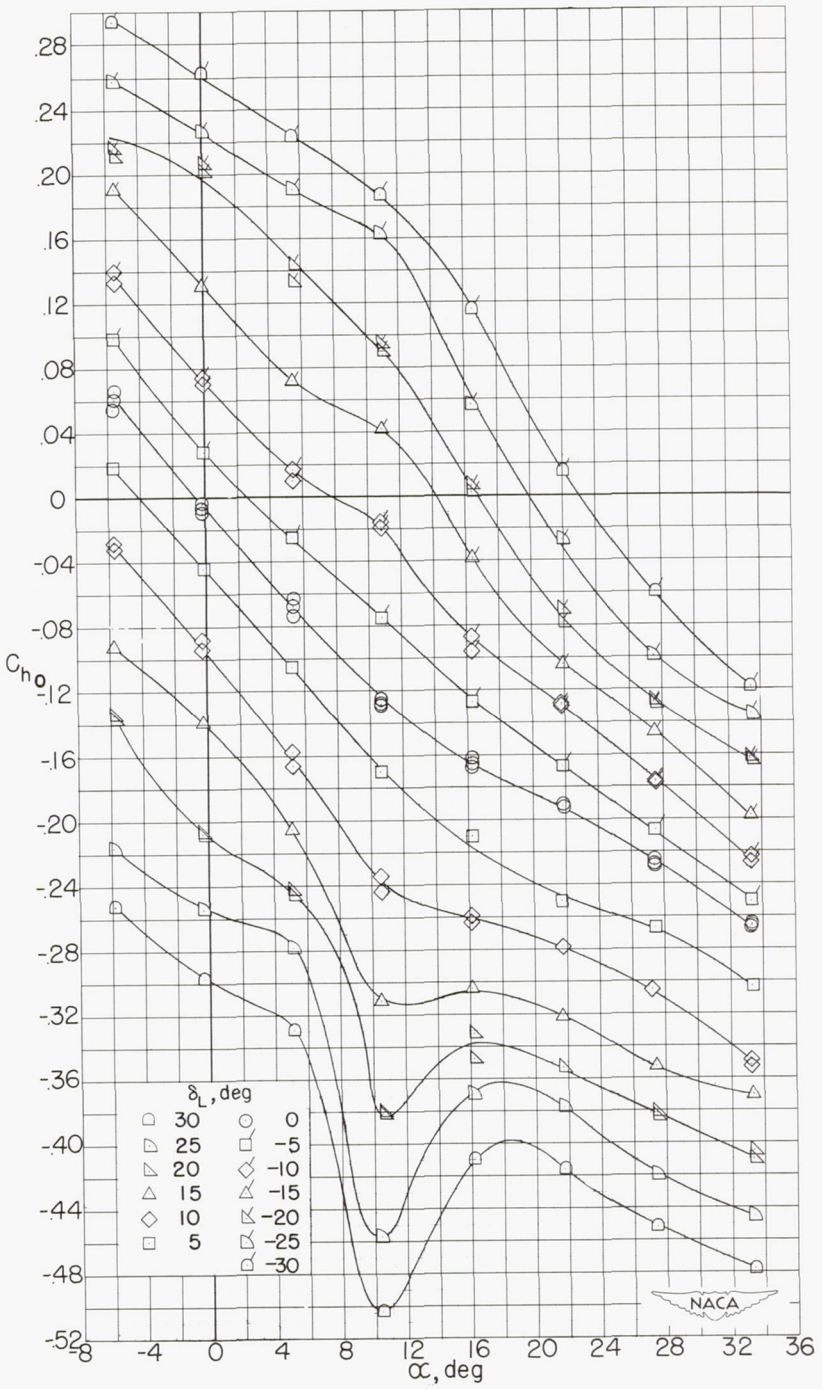

(a) Outboard ailavator deflected alone.

Figure 14.- Effect of left ailavator deflection on the hinge-moment characteristics of the basic wing configuration.

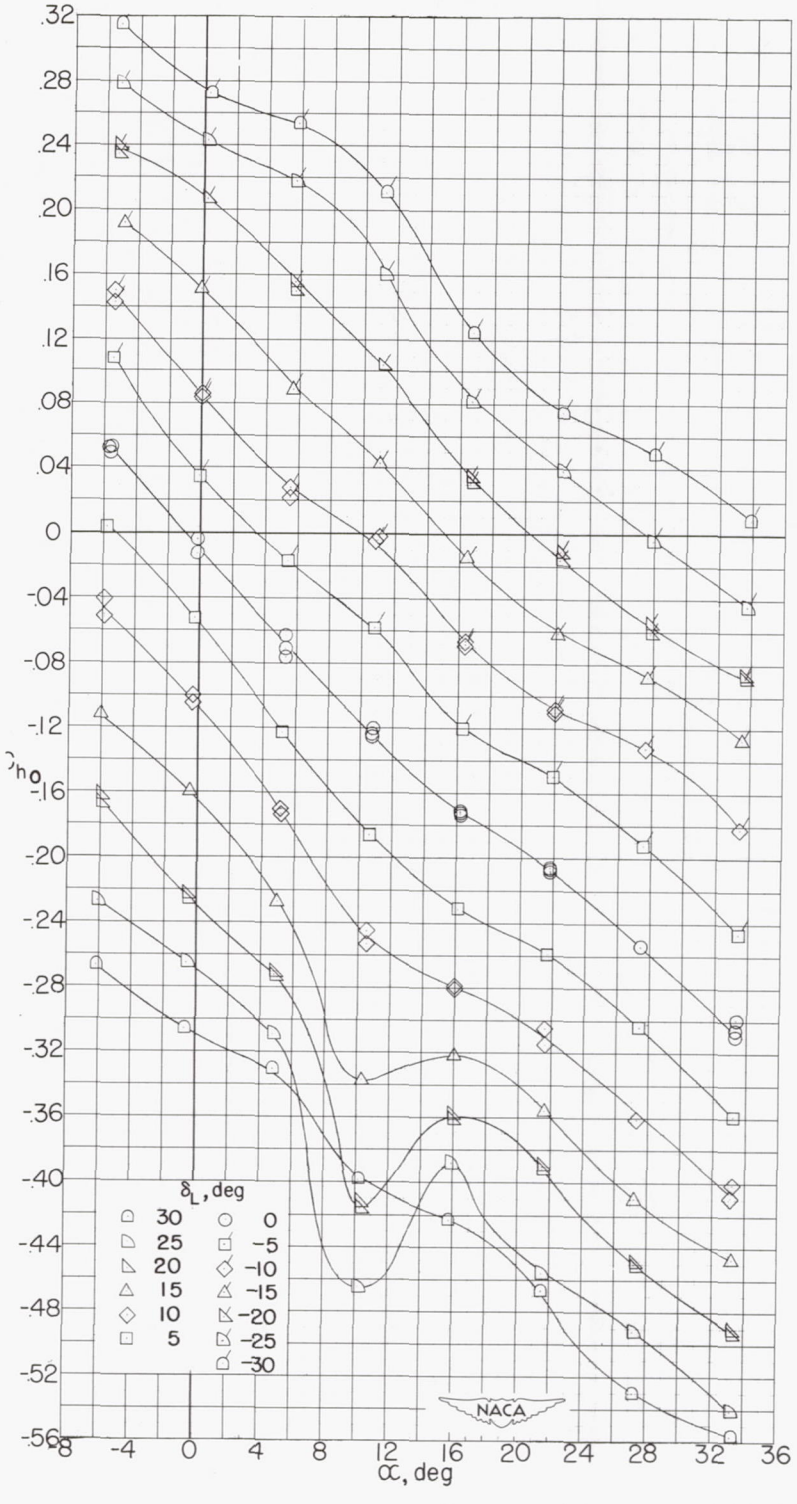

(b) Outboard ailavator deflected in combination with inboard ailavator.

Figure 14.- Continued.

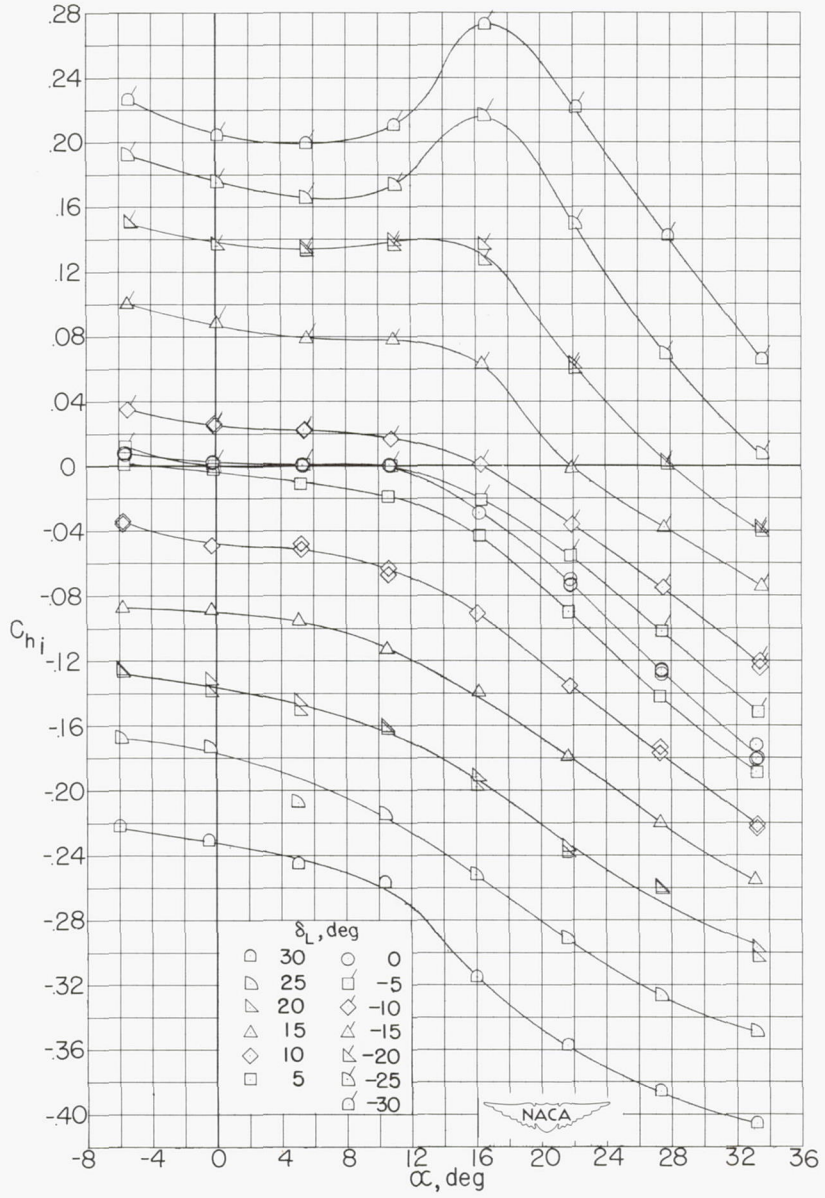

(c) Inboard ailavator deflected alone.

Figure 14.- Continued.

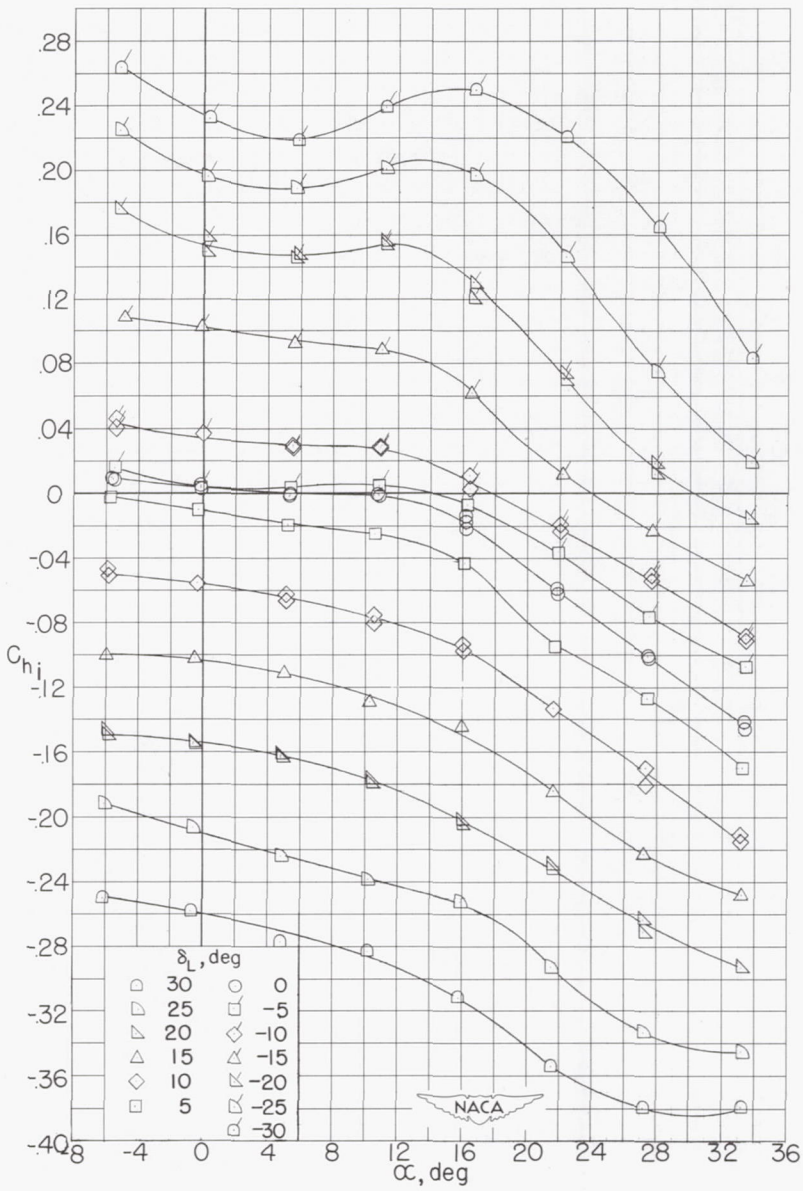

(d) Inboard ailavator deflected in combination with outboard ailavator.

Figure 14.- Concluded.

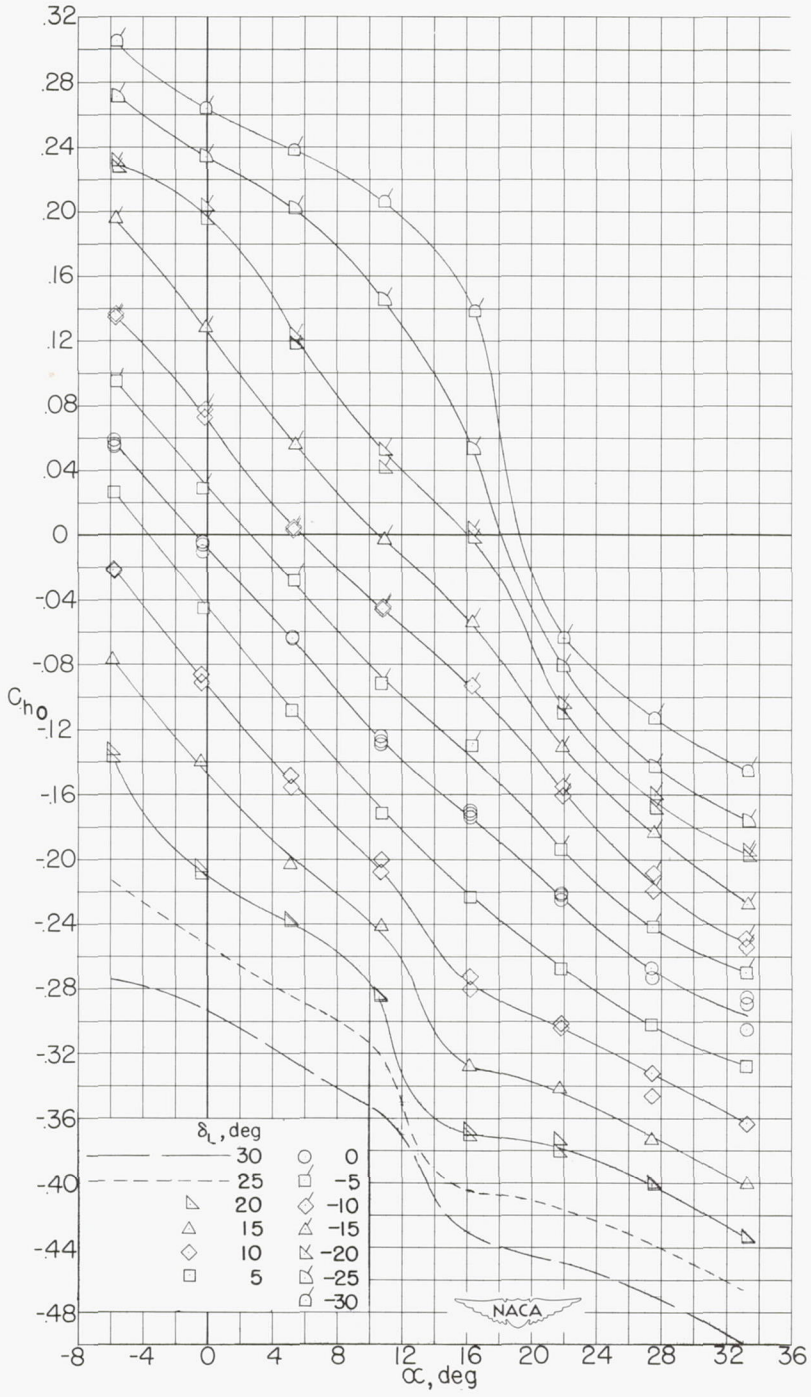

(a) Outboard ailavator deflected alone.

Figure 15.- Effect of left ailavator deflection on the hinge-moment characteristics of the round-nose wing configuration.

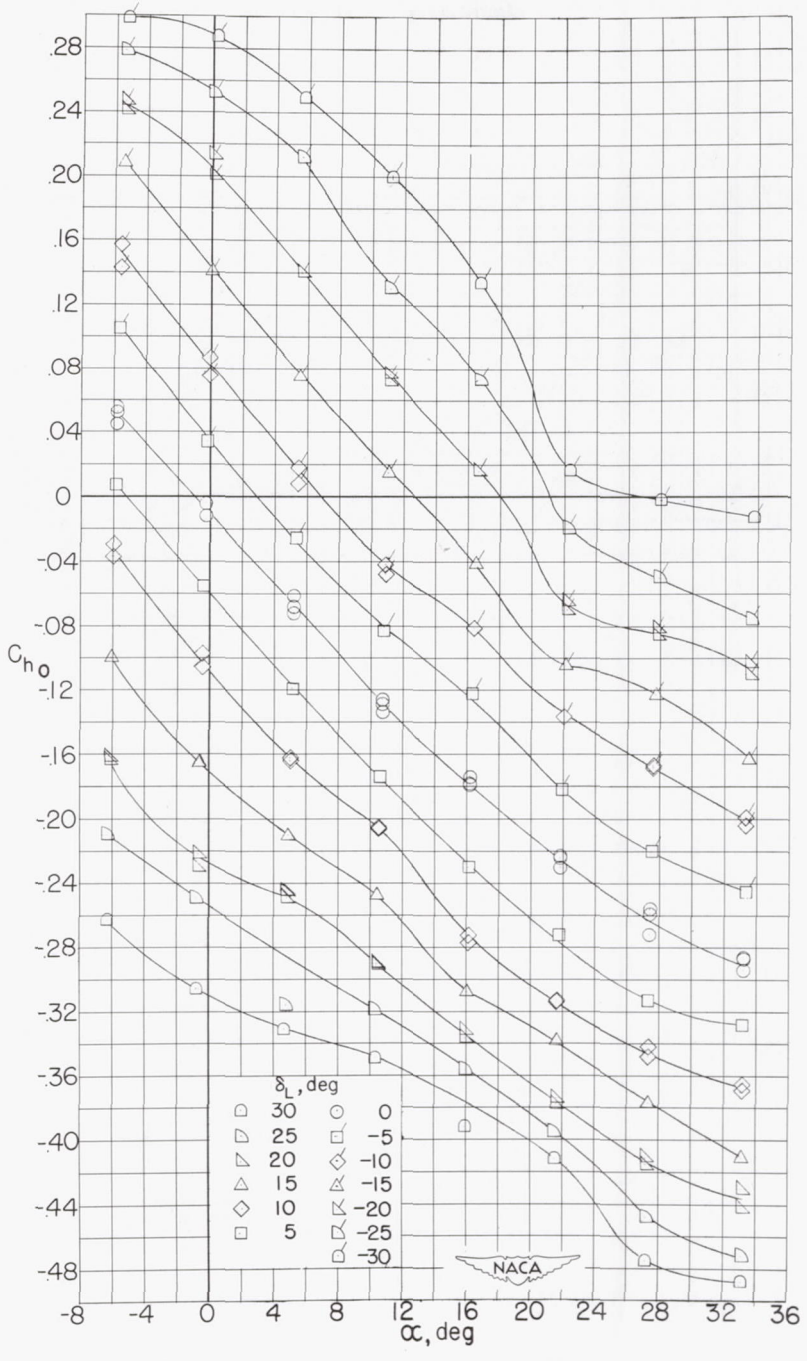

(b) Outboard ailavator deflected in combination with inboard ailavator.

Figure 15.- Continued.

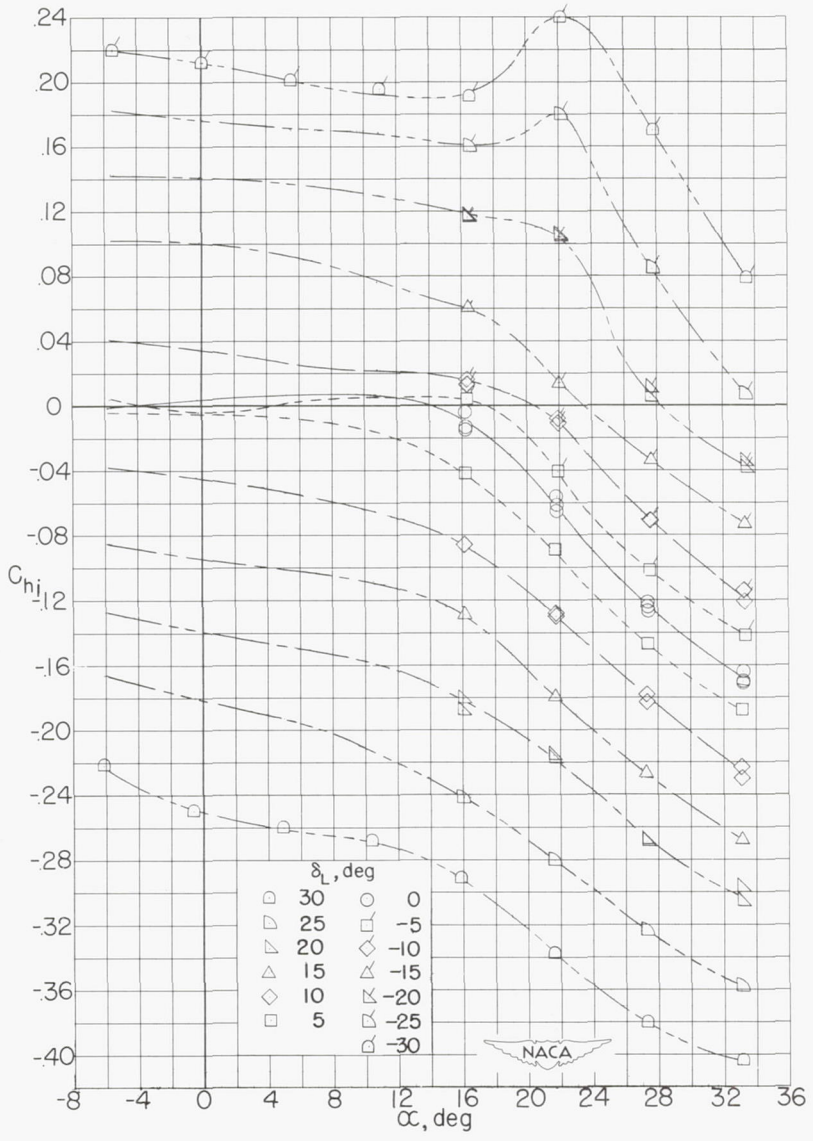

(c) Inboard ailavator deflected alone.

Figure 15.- Continued.

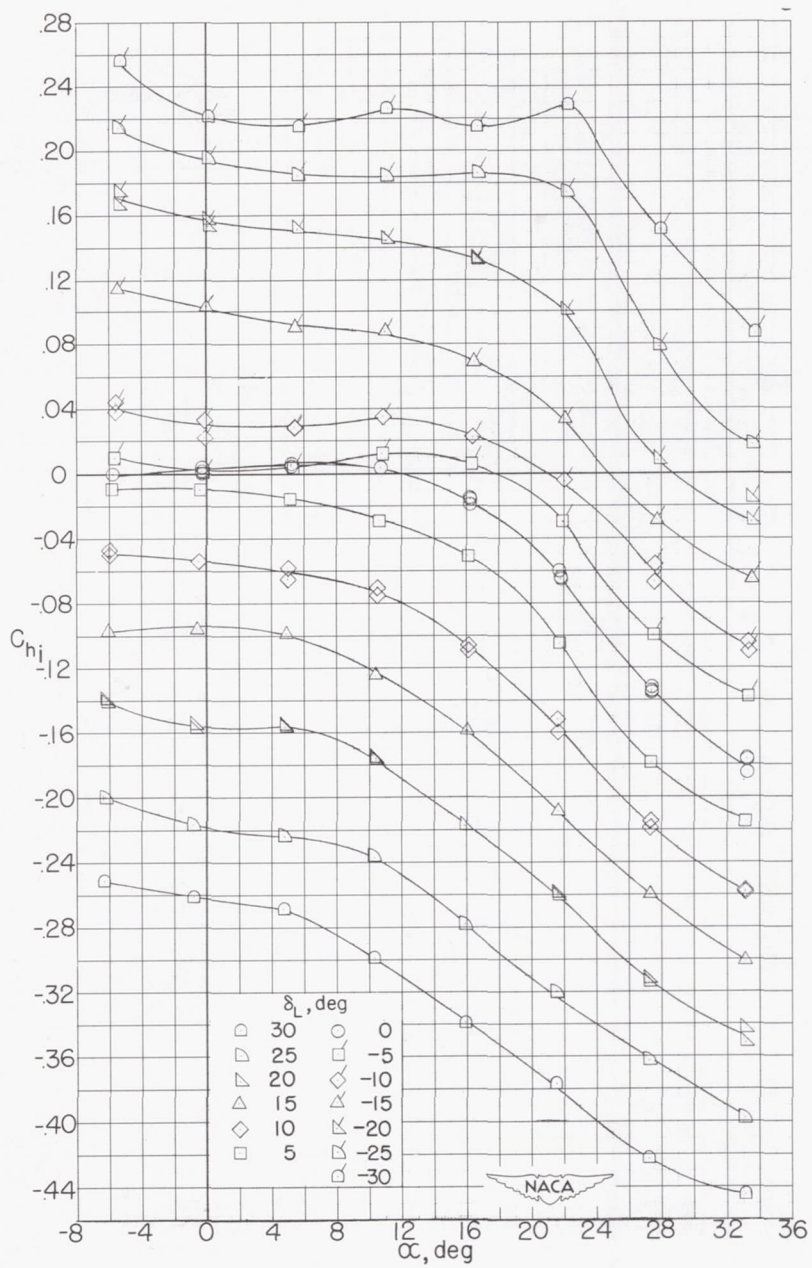

(d) Inboard ailavator deflected in combination with outboard ailavator.

Figure 15.- Concluded.

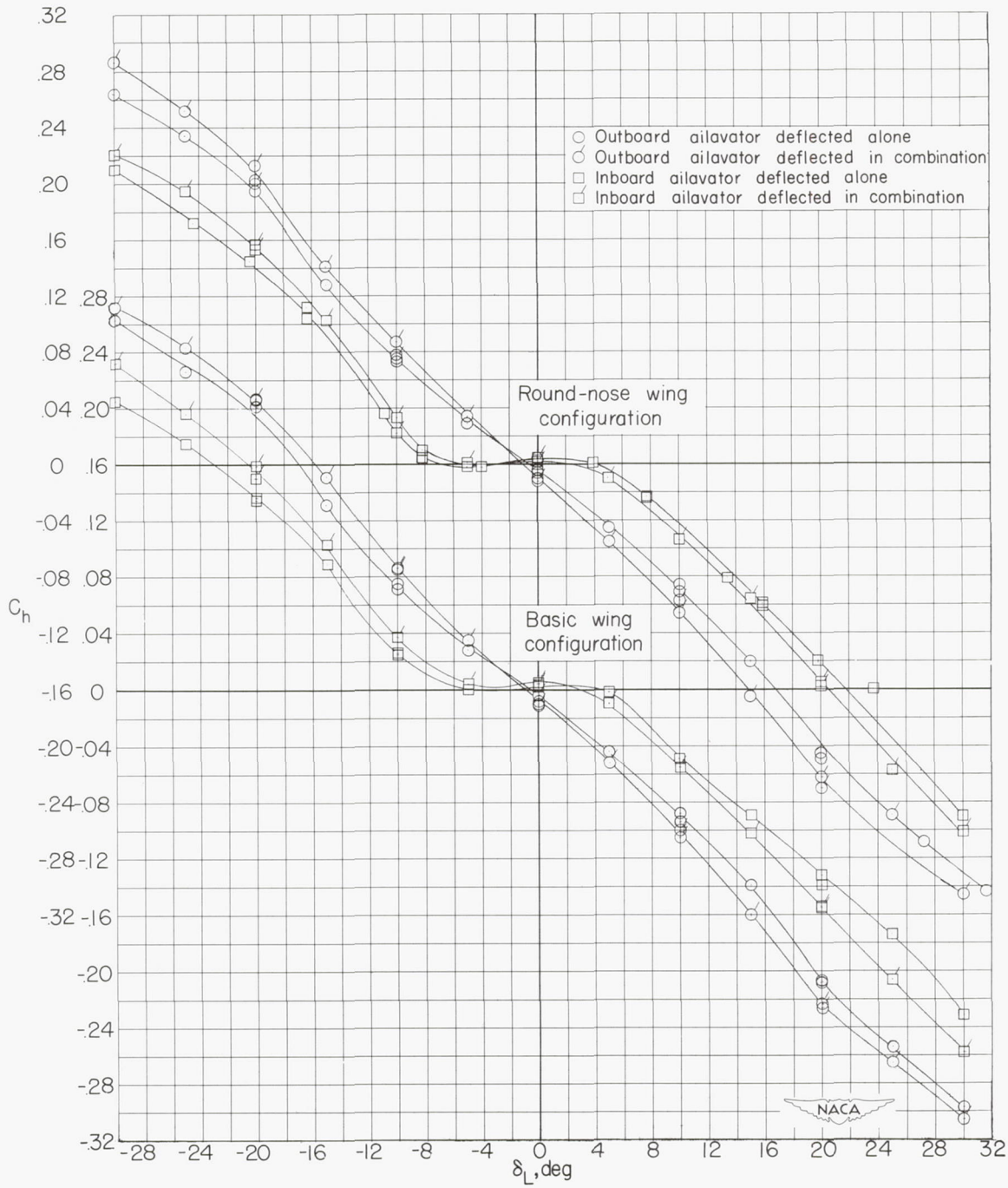

Figure 16.- Effect of ailavator plan form on the variation of C_h with δ_L for the basic and round-nose wing configurations at zero uncorrected angle of attack.

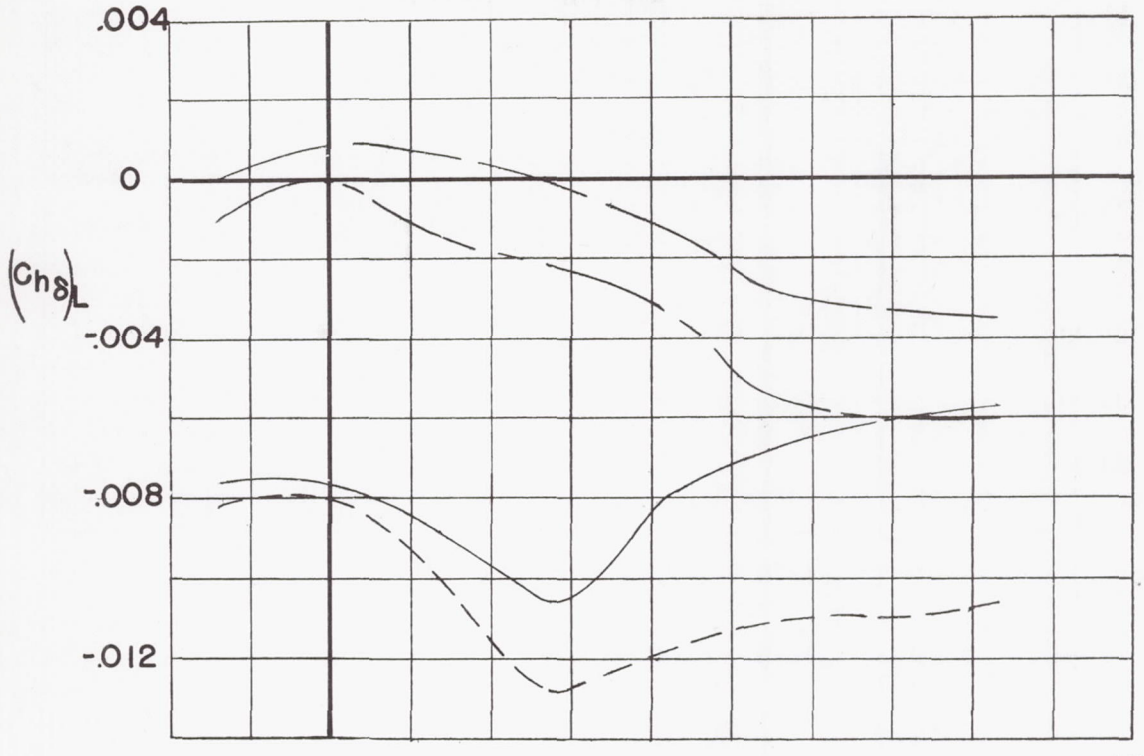

(a) Basic wing configuration.

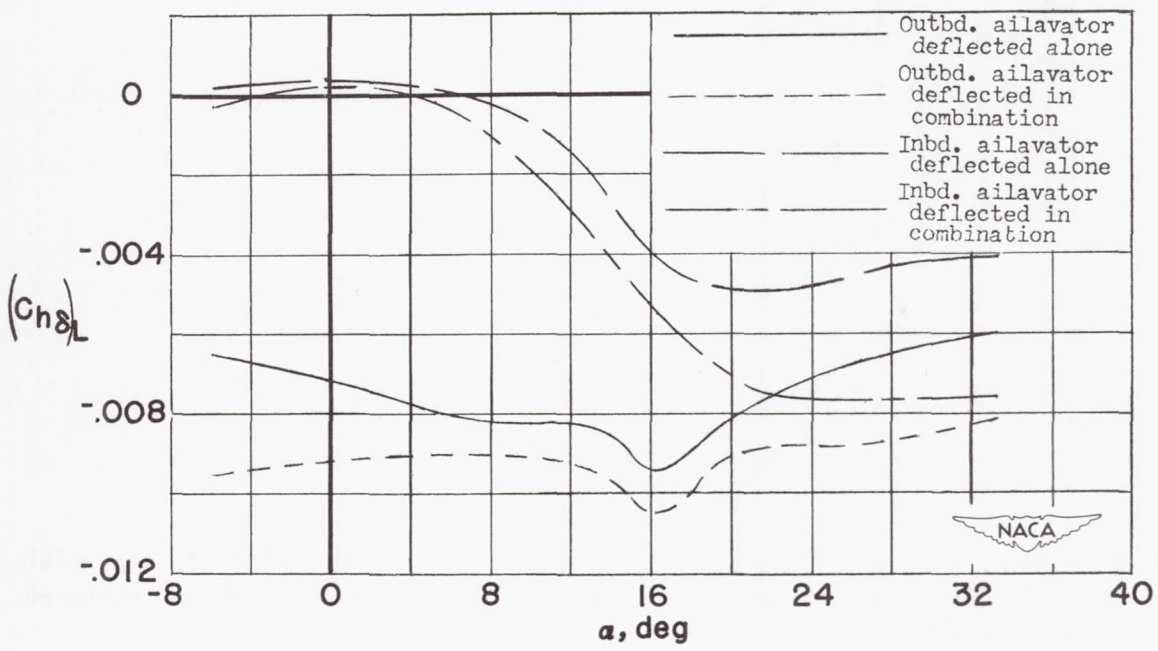

(b) Round-nose wing configuration.

Figure 17.- Variation of $(C_{h_\delta})_L$ with α. ($(C_{h_\delta})_L$ measured at $\delta_L = 0^\circ$.)